Title

PeRL: a circum-Arctic Permafrost Region Pond and Lake database

Journal

Earth System Science Data, 9(1)

ISSN

1866-3508

Authors

Muster, Sina

Roth, Kurt

Langer, Moritz

et al.

Publication Date

2017

DOI

10.5194/essd-9-317-2017

Peer reviewed

Earth Syst. Sci. Data, 9, 317–348, 2017
https://doi.org/10.5194/essd-9-317-2017

Open Access Earth System Science Data

PeRL: a circum-Arctic Permafrost Region Pond and Lake database

Sina Muster[1], Kurt Roth[2], Moritz Langer[3], Stephan Lange[1], Fabio Cresto Aleina[4], Annett Bartsch[5], Anne Morgenstern[1], Guido Grosse[1], Benjamin Jones[6], A. Britta K. Sannel[7], Ylva Sjöberg[7], Frank Günther[1], Christian Andresen[8], Alexandra Veremeeva[9], Prajna R. Lindgren[10], Frédéric Bouchard[11,13], Mark J. Lara[12], Daniel Fortier[13], Simon Charbonneau[13], Tarmo A. Virtanen[14], Gustaf Hugelius[7], Juri Palmtag[7], Matthias B. Siewert[7], William J. Riley[15], Charles D. Koven[15], and Julia Boike[1]

[1]Alfred Wegener Institute Helmholtz Centre for Polar and Marine Research, Telegrafenberg A43, 14473 Potsdam, Germany
[2]Institute for Environmental Physics, Heidelberg University, Heidelberg, Germany
[3]Humboldt University, Berlin, Germany
[4]Max Planck Institute for Meteorology, Hamburg, Germany
[5]Zentralanstalt für Meteorologie and Geodynamik, Vienna, Austria
[6]U.S. Geological Survey – Alaska Science Center, Anchorage, AK 99508, USA
[7]Stockholm University, Department of Physical Geography and the Bolin Centre for Climate Research, 10691 Stockholm, Sweden
[8]Los Alamos National Laboratory, Los Alamos, NM, USA
[9]Institute of Physicochemical and Biological Problems in Soil Science, Russian Academy of Sciences, Pushchino, Russia
[10]Geophysical Institute, University of Alaska Fairbanks, Fairbanks, AK, USA
[11]Institut national de la recherche scientifique (INRS), Centre Eau Terre Environnement (ETE), Québec QC, G1K 9A9, Canada
[12]Department of Plant Biology, University of Illinois at Urbana-Champaign, Urbana, IL 61801, USA
[13]Geography Department, University of Montréal, Montréal QC, H3C 3J7, Canada
[14]Department of Environmental Sciences, University of Helsinki, Helsinki, Finland
[15]Climate and Ecosystem Sciences Division, Lawrence Berkeley National Laboratory, Berkeley, USA

Correspondence to: Sina Muster (sina.muster@awi.de)

Received: 15 November 2016 – Discussion started: 22 November 2016
Revised: 27 March 2017 – Accepted: 1 April 2017 – Published: 6 June 2017

Abstract. Ponds and lakes are abundant in Arctic permafrost lowlands. They play an important role in Arctic wetland ecosystems by regulating carbon, water, and energy fluxes and providing freshwater habitats. However, ponds, i.e., waterbodies with surface areas smaller than 1.0×10^4 m^2, have not been inventoried on global and regional scales. The Permafrost Region Pond and Lake (PeRL) database presents the results of a circum-Arctic effort to map ponds and lakes from modern (2002–2013) high-resolution aerial and satellite imagery with a resolution of 5 m or better. The database also includes historical imagery from 1948 to 1965 with a resolution of 6 m or better. PeRL includes 69 maps covering a wide range of environmental conditions from tundra to boreal regions and from continuous to discontinuous permafrost zones. Waterbody maps are linked to regional permafrost landscape maps which provide information on permafrost extent, ground ice volume, geology, and lithology. This paper describes waterbody classification and accuracy, and presents statistics of waterbody distribution for each site. Maps of permafrost landscapes in Alaska, Canada, and Russia are used to extrapolate waterbody statistics from the site level to regional landscape units. PeRL presents pond and lake estimates for a total area of

1.4×10^6 km^2 across the Arctic, about 17 % of the Arctic lowland (< 300 m a.s.l.) land surface area. PeRL waterbodies with sizes of 1.0×10^6 m^2 down to 1.0×10^2 m^2 contributed up to 21 % to the total water fraction. Waterbody density ranged from 1.0×10 to 9.4×10^1 km^{-2}. Ponds are the dominant waterbody type by number in all landscapes representing 45–99 % of the total waterbody number. The implementation of PeRL size distributions in land surface models will greatly improve the investigation and projection of surface inundation and carbon fluxes in permafrost lowlands. Waterbody maps, study area boundaries, and maps of regional permafrost landscapes including detailed metadata are available at https://doi.pangaea.de/10.1594/PANGAEA.868349.

1 Introduction

Globally, Arctic lowlands underlain by permafrost have both the highest number and area fraction of waterbodies (Lehner and Döll, 2004; Grosse et al., 2013; Verpoorter et al., 2014). These landscapes play a key role as a freshwater resource, as habitat for wildlife, and as part of the water, carbon, and energy cycles (Rautio et al., 2011; CAFF, 2013). The rapid warming of the Arctic affects the distribution of surface and subsurface water due to permafrost degradation and increased evapotranspiration (Hinzman et al., 2013). Remote-sensing studies have found both increasing and decreasing trends in surface water extent for waterbodies in permafrost regions across broad spatial and temporal scales (e.g., Carroll et al., 2011; Watts et al., 2012; Boike et al., 2016; Kravtsova and Rodionova, 2016). These studies, however, are limited in their assessment of changes in surface inundation since they only include lakes, i.e., waterbodies with a surface area of 1.0×10^4 m^2 or larger. Ponds with a surface area smaller than 1.0×10^4 m^2, on the other hand, have not yet been inventoried on the global scale. Yet ponds dominate the total number of waterbodies in Arctic lowlands, accounting for up to 95 % of individual waterbodies, and may contribute up to 30 % to the total water surface area (Muster et al., 2012; Muster, 2013). Arctic ponds are characterized by intense biogeophysical and biogeochemical processes. They have been identified as a large source of carbon fluxes compared to the surrounding terrestrial environment (Rautio et al., 2011; Laurion et al., 2010; Abnizova et al., 2012; Langer et al., 2015; Wik et al., 2016; Bouchard et al., 2015). Due to their small surface areas and shallow depths, ponds are especially prone to change; various studies reported ponds drying out or increasing in abundance due to new thermokarst or the drainage of large lakes (Jones et al., 2011; Andresen and Lougheed, 2015; Liljedahl et al., 2016). Such changes in surface inundation may significantly alter regional water, energy, and carbon fluxes (Watts et al., 2014; Lara et al., 2015). Both the monitoring and modeling of pond and lake development are therefore crucial to better understand the trajectories of Arctic land cover dynamics in relation to climate and environmental change. Currently, however, the direction and magnitude of these changes remain uncertain, mainly due to the limited extent of high-resolution studies and the lack of pond representation in global databases. Although recent efforts have produced global land cover maps with resolutions of 30 m (Liao et al., 2014; Verpoorter et al., 2014; Feng et al., 2015; Paltan et al., 2015), these data sets only include lakes.

To complement previous approaches, we present the Permafrost Region Pond and Lake (PeRL) database, a circum-Arctic effort that compiles 69 maps of ponds and lakes from remote-sensing data with high spatial resolution (of ≤ 6 m) (Fig. 1). This database fills the gap in available global databases that have cutoffs in waterbody surface area at 1.0×10^4 m^2 or above. In addition, we link PeRL waterbody maps with existing maps of permafrost landscapes to extrapolate waterbody distributions from the individual study areas to larger landscapes units. Permafrost landscapes are terrain units characterized by distinct properties such as climate, surficial geology, parent material, permafrost extent, ground ice content, and topography. These properties have been identified as major factors in the evolution and distribution of northern waterbodies (Smith et al., 2007; Grosse et al., 2013; Veremeeva and Glushkova, 2016).

The core objectives of the PeRL database are to (i) archive and disseminate fine-resolution geospatial data of northern high-latitude waterbodies, (ii) quantify the intra- and interregional variability in waterbody size distributions, and (iii) provide regional key statistics, including the uncertainty in waterbody distributions, that can be used to benchmark site-, regional-, and global-scale land models.

2 Definition of ponds and lakes

The definition of ponds and lakes varies in the literature and depends on the chosen scale and goal of studies when characterizing waterbodies. The Ramsar classification scheme defines ponds as permanently inundated basins smaller than 8.0×10^4 m^2 in surface area (Ramsar Convention Secretariat, 2010). Studies have also used surface areas smaller than 5.0×10^4 m^2 (Labrecque et al., 2009) or 1.0×10^4 m^2 (Rautio et al., 2011) to distinguish ponds from lakes.

In remote-sensing studies, surface area is the most reliably inferred parameter related to waterbody properties. Physical and biogeochemical processes of waterbodies, however, also strongly depend on waterbody depth. Differences in thermodynamics are associated with water depth, where deeper lakes may develop a stratified water column while shallow

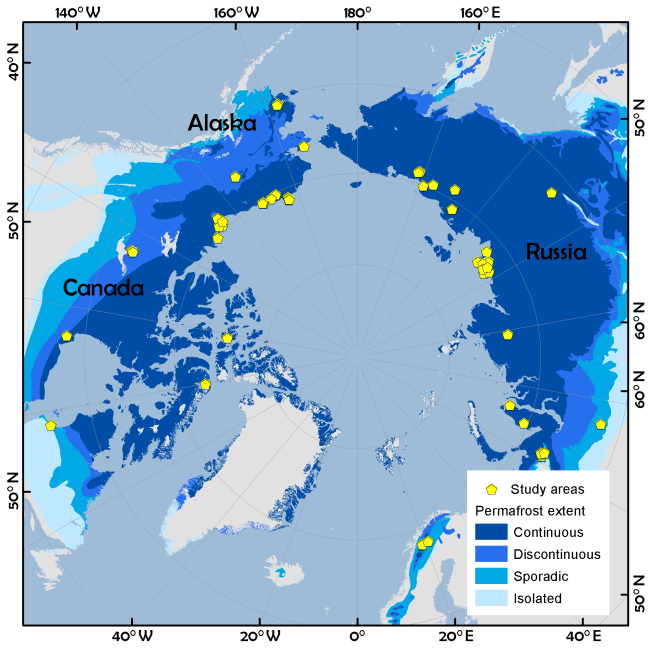

Figure 1. Distribution of PeRL study areas. Permafrost extent according to Brown et al. (1998).

ponds remain well mixed. In high latitudes, waterbodies with depths greater than 2 m are likely to remain unfrozen at the bottom throughout winter, thus providing overwintering habitat for fish and other aquatic species. In permafrost regions, a continuously unfrozen layer (talik) may develop underneath such deeper waterbodies, which strongly affects carbon cycling in these sediments (Schuur et al., 2008). Several studies have shown a positive correlation between waterbody surface area and depth (Langer et al., 2015; Wik et al., 2016). However, there is large variability in the area–depth relationship, i.e., there are large but shallow lakes that freeze to the bottom and small but deep ponds that develop a talik, and these characteristics may also change over time with changes in water level and basin morphology. In this study we distinguish ponds and lakes based on their surface area. We adopt the distinction of Rautio et al. (2011) and define ponds as bodies of largely standing water with a surface area smaller than 1.0×10^4 m^2 and lakes as waterbodies with a surface area of 1.0×10^4 m^2 or larger.

3 PeRL database generation

3.1 Data sources and processing

PeRL's goal is to make high-resolution waterbody maps available to a large science community. PeRL compiles both previously published and unpublished fine-scale waterbody maps. Maps were included if they met the resolution criteria of 5 m or less for modern imagery and 6 m for historical imagery. Historical imagery was included to enable high-resolution change detection in ponds and lakes.

Twenty-nine maps were specifically produced for PeRL to complement the published maps in order to represent a broad range of landscape types with regard to permafrost extent, ground ice content, geology, and ecozone. All waterbody maps were derived from optical or radar airborne or satellite imagery that were acquired between mid and late summer (July–September), thereby excluding the snowmelt and early summer season. Modern imagery dates from 2002 to 2013, and historical imagery dates from 1948 to 1965. Previously published maps are the product of many independent studies, which leads to a broad range of image types and classification methods used. Details on image processing and classification procedures for already published maps ($n = 31$) are listed in Table A1 and the respective publications. The processing of new PeRL maps is described in Sect. 3.2.

3.2 PeRL image processing and classification

3.2.1 Image processing

Available high-resolution imagery used for PeRL map production included optical aerial and satellite imagery (GeoEye, QuickBird, WorldView-1 and -2, and the Korean Multi-Purpose Satellite 2 (KOMPSAT-2)) and radar (TerraSAR-X) imagery.

Most optical imagery provided a near-infrared band that was used for classification, with the exception of WorldView 1, which only has a panchromatic band. Preprocessing of the optical imagery involved georeferencing or orthorectification depending on the availability of high-resolution digital elevation models (Appendix A, Table A1).

TerraSAR-X (TSX) imagery was acquired in Stripmap Mode with an HH polarization as the geocoded Enhanced Ellipsoid Corrected (EEC) product or as the Single Look Slant Range Complex (SSC) product which was then processed to EEC (Sect. A1). TSX images were filtered in ENvironment for Visualizing Images (ENVI) v4.7 (ITTVIS) in order to reduce image noise using a lee filter with a 3×3 pixel window followed by a gamma filter with a 7×7 or 11×11 window depending on the image quality (Klonus and Ehlers, 2008).

3.2.2 Classification of open water

Imagery was classified using either a density slice or an unsupervised *k*-means classification in ENVI v4.8 (ITTVIS). The panchromatic, the near-infrared, and the X-Band (HH polarization) show a sharp contrast between open water and surrounding vegetation. Visual inspection of the imagery could therefore be used to determine individual threshold values (in the case of density slice) or to assign classes (in the case of *k*-means unsupervised classification) for the extraction of open-water surfaces. Threshold values and class boundaries varied between images and sites due to differences in illumination, acquisition geometry, and radiometric properties

of images. Detailed information on remote-sensing imagery and the classification procedure for each site is listed in Appendix A (Table A1).

The classification procedure in ENVI produces raster images that were converted to ESRI vector files so that each waterbody is represented as a single polygon. Vector files were then manually processed in ArcGIS v10.2 (ESRI) to fill gaps in waterbody surfaces and remove streams, rivers, and shadows due to clouds or topography and partial lakes along the study area boundaries. The minimum waterbody size was set to at least 4 pixels. This equals less than 4 m^2 for the highest resolutions of less than 1 m and 64 m^2 for the lowest resolution of 4 m for modern imagery (1.4×10^2 m^2 for historical imagery with resolutions of 6 m). All classified objects smaller than the minimum size were removed. Partial lakes along the study area boundaries, segments of streams and rivers, and shadows due to clouds or topography were manually removed.

3.3 Study area boundaries

Each waterbody map is associated with a vector file that delineates the study area's boundary. Boundaries were calculated for each map – whether new or previously published – in ArcGIS by first producing a positive buffer of 1–3 km around each waterbody in the map and merging the individual buffers into one single polygon. From that single polygon we then subtracted the same distance again, which rendered the study area boundary. The area of the boundary is referred to as the total mapped extent of that site (Table 1). For sites with multi-temporal data, the total mapped extent of the oldest classification was chosen as a reference in order to calculate changes in pond and lake statistics over time.

4 PeRL statistical analysis

Statistics such as areal fraction of water or average waterbody surface area are meaningful measures to compare waterbody distributions between individual study areas and permafrost landscapes. Statistics were calculated for all waterbodies, as well as separately for ponds and lakes. We calculated areal fraction, i.e., the area fraction of water relative to land (the total mapped area), and waterbody density, i.e., the number of waterbodies per kilometer for each site, using the software package R version 3.3.1. However, statistics are subject to the size of the study area. Very small study areas may not capture larger waterbodies, which may nonetheless be characteristic of the larger landscape. Very large study areas, on the other hand, may show more spatial variation in waterbody distribution than smaller study areas. In order to make statistics comparable between study areas, we subdivided larger study areas into boxes of 10 km × 10 km. The box size was chosen as a function of the standard error (Sect. A2). We calculated the statistics for each box and then averaged the statistics across all boxes within each study area. This subgrid analysis was conducted for all study areas larger than 300 km^2 for which at least four boxes could be sampled.

Statistics are also subject to image resolution, which defines the minimum object size that can be confidently mapped. For all modern imagery, the minimum waterbody size included in the calculation of statistics was therefore set to 1.0×10^2 m^2 (1.4×10^2 m^2 for historical imagery). Very large lakes are not representative of all study areas and may only be partially mapped within a 10 km × 10 km box. We therefore chose a maximum waterbody size of 1.0×10^6 m^2 to be included in the calculation of statistics.

5 Extrapolation of site-level waterbody statistics to permafrost landscapes

5.1 Regional maps of permafrost landscapes

Waterbody statistics of each site were extrapolated to permafrost landscapes based on the assumption that distributions of ponds and lakes are similar for similar permafrost landscapes, i.e., areas with similar properties regarding climate, geology, lithology (soil texture), permafrost extent, and ground ice volume. Vector maps of permafrost landscapes (PLM) are available on the regional level: the Alaskan map of permafrost characteristics (AK2008) (Jorgenson et al., 2008a), the National Ecological Framework for Canada (NEF) (Marshall et al., 1999), and the Land Resources of Russia (LRR) (Stolbovoi and McCallum, 2002). Despite differences in mapping approaches and terminology, these databases report similar landscape characteristics on comparable scales. All regional maps were available as vector files, which were converted to a common North Pole Lambert Azimuthal Equal-Area (NPLAEA) projection. All PLM were clipped in ArcGIS v10.4 with a lowland mask including only areas with elevations of 300 m or lower. The lowland mask was derived for the entire Arctic using the digital elevation model GTOPO30 (USGS). Details on the properties of each PLM are provided in Appendix B. The original PLM were merged in ArcGIS to produce a unified circum-Arctic vector file and map representation. Landscape attributes that were retained from the original PLM were ecozone, permafrost extent, ground ice volume, surficial geology, and lithology. Variable names were consolidated using uniform variable names (Appendix B, Table B4).

5.2 Extrapolation of waterbody statistics to permafrost landscapes

Waterbody maps were spatially linked with their associated permafrost landscape. Maps within the same landscape were combined, whereas maps spanning two or more landscapes were divided by selecting all waterbodies that intersected with the respective permafrost landscape. If several maps were present within one permafrost landscape unit they were combined and average statistics calculated across all maps in

that unit. Historical maps and unedited classifications were not used in the extrapolation.

Extrapolations were done in Alaska, Canada, and Russia for waterbody maps with a (combined) extent of 100 km^2 or larger but not for Europe where available waterbody maps were too small. Maps in the Canadian high Arctic were smaller than 1.0×10^2 km^2 but represent typical wetlands in that region and were therefore included in the extrapolation. Figures D1, D2, D3, and D4 show the location of waterbody maps within their associated permafrost landscape.

Extrapolated statistics were assigned two confidence classes: (1) high and (2) low confidence. Permafrost landscapes were assigned to the high confidence class if a map was present in the permafrost landscape of that ecozone. The low confidence class indicates that statistics were derived from the same permafrost landscape but in a different ecozone. Due to differences in the mapping and generalization of landscape properties of the regional PLM, the extrapolation was conducted only within each region.

6 PeRL database features

The database provides two different map products: (i) site-level waterbody maps and (ii) an extrapolated circum-Arctic waterbody map. The database also provides different tables which present statistical parameters for each individual waterbody map (Appendix B) and aggregated statistics for permafrost landscape (PL) units in the circum-Arctic map (Table 3).

6.1 Site-level waterbody maps

6.1.1 Data set structure

Altogether, the database features 70 individual waterbody maps as ESRI shape files. Each waterbody shape file is named according to a map ID. The map ID consists of a three-letter abbreviation of the site name, followed by a running three-digit number and the acquisition date of the base imagery (YYYY-MM-DD). Vector files were projected to the NPLAEA projection. The area and perimeter of each waterbody and site were calculated in ArcGIS 10.4 in square meters. Each vector file is accompanied by an xml-file which lists metadata about classification and references as presented in Tables 1 and A1. Each map has a polygon associated with it that contains the study area, i.e., the total land area of the waterbody map. All study area boundaries are stored in the file PeRL_study_areas.shp and can be identified via the map ID (Table C2). The study area shape file also includes the site characteristics listed in Table 2.

Fifty-eight maps are considered "clean", i.e., they have been manually edited to include only ponds and lakes (Table 1). Eight maps are "clean with partial waterbodies". These are multi-temporal maps with very small map extents where partial waterbodies along the study area boundary were not deleted in order to retain information for change detection analysis. Four maps were not manually edited due to their very large map extent and may include partial waterbodies, streams, rivers, or shadows.

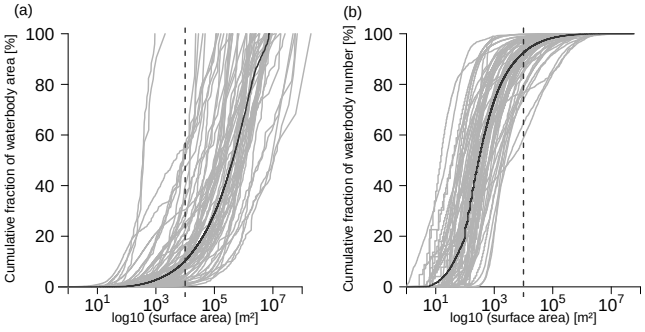

Figure 2. Empirical cumulative distribution function of waterbody area **(a)** and waterbody number **(b)**. Grey lines represent individual sites across all regions. Black lines represent the mean function averaged over all sites. Vertical dashed line in each panel represents the pond–lake size threshold used in this paper.

6.1.2 Spatial and environmental characteristics

PeRL study areas are widely distributed throughout Arctic lowlands in Alaska, Canada, Russia, and Europe and cover a latitudinal gradient of about 20° (55.3–75.7° N), including tundra to boreal regions, and they are located in continuous, discontinuous, and sporadic permafrost zones (Fig. 1). Mean annual temperature ranges from 0 to −20 °C, and average annual precipitation ranges from 97 to 650 mm (Table 1). Twenty-one sites are located in Alaska, covering a total area of 7.3×10^3 km^2. Canada has 14 sites covering 6.4×10^3 km^2, and Russia has 30 sites covering 2.9×10^3 km^2 in total. Four sites are located in Sweden, with a total mapped area of 41 km^2. Individual map extents range from 0.2 to 9825.7 km^2, with a mean of 622.8 km^2 (Table 1). The database includes six multi-temporal classifications in the Kotzebue Sound lowlands and on the Barrow Peninsula in Alaska (Andresen and Lougheed, 2015), on the Grande Rivière de la Baleine Plateau (Bouchard et al., 2014) and in the Hudson Bay Lowlands in Canada, in Lapland in Sweden, and in the Usa River basin in Russia (Hugelius et al., 2011; Sannel and Kuhry, 2011). Ponds contributed about 45–99 % of the total number of waterbodies, with a mean of 85 ± 14 %, and up to 34 % to the total water surface area, with a mean of 12 ± 8.3 % (Fig. 2 and Appendix E). The water fraction of the total mapped area ranged from about 1 to 21 % for all waterbodies and from > 1 to 6 % for ponds. Waterbody density per square kilometer ranged from 1.0×10 km^{-2} in the Indigirka lowlands, Russia, to 9.4×10^1 km^{-2} in the Olenek Channel of the Lena Delta (Table E4).

Table 1. Characteristics of waterbody maps. A "clean" map state indicates that the map only includes ponds or lakes. A "raw" map state indicates that no manual editing was conducted and that the map may contain rivers, streams, partial waterbodies, or cloud shadows. References indicate whether the map has already been published or was produced specifically for PeRL.

Map ID	Map extent	Resolution (m)	Accuracy	Classes	Min. size (m^2)	State	Reference
abi0012010xxxx	38.4	1.0	> 0.71	open water	30.0	clean	this paper
arg00120110829	195.9	4.0	NA	open water	64.0	clean	this paper
arg0022009xxxx	5023.6	5.0	0.85	open water	100.0	raw	Bartsch and Seifert (2012)
arg00320110711	223.7	4.0	NA	open water	64.0	clean	this paper
bar00119480804	19.0	0.7	NA	open water	16.0	clean	Andresen and Lougheed (2015)
bar00120020802	19.0	0.7	NA	open water	16.0	clean	Andresen and Lougheed (2015)
bar00120080730	19.0	0.7	NA	open water	16.0	clean	Andresen and Lougheed (2015)
bar00120100810	19.0	0.5	0.93	open water	16.0	clean	Andresen and Lougheed (2015)
byk00120060709	170.2	2.5	NA	open water	30.0	clean	Grosse et al. (2008)
byl00120160728	45.3	0.5	0.77	open water	16.0	clean	this paper
che00120020709	220.8	1.0	NA	open water	30.0	clean	Grosse et al. (2008)
che00220090724	340.3	3.0	0.97	open water	36.0	clean	Widhalm et al. (2014a, b)
elc00120090825	126.0	2.5	NA	open water, water with emersed vegetation	25.0	clean	this paper
elc00220020801	143.2	0.6	0.89–0.95	open water	7.8	clean	Lara et al. (2015)
elc00320090802	51.4	4.0	NA	open water	64.0	clean	Muster et al. (2013)
elc004200808xx		0.6	> 0.75	troughs with open water	1.5	clean	Lara et al. (2015)
esk00120090727	923.4	2.5	NA	open water	36.0	clean	this paper
fir00120090906	150.0	4.0	NA	open water	64.0	clean	this paper
fir0022009xxxx	9825.7	5.0	0.85	open water	100.0	raw	Bartsch and Seifert (2012)
fis00120020715	236.8	1.3	NA	open water	100.0	clean	Jones et al. (2013)
grp00119590707	0.2	0.4	NA	open water	17.0	clean	Bouchard et al. (2014)
grp00120060707	0.2	0.61	NA	open water	13.0	clean	Bouchard et al. (2014)
hbl00119540701	4.0	1.0	NA	open water	51.0	clean with partial waterbodies	Sannel and Brown (2010), Sannel and Kuhry (2011)
hbl00119740617	4.0	1.0	NA	open water	47.5	clean with partial waterbodies	Sannel and Brown (2010), Sannel and Kuhry (2011)
hbl00120060706	4.0	0.6	NA	open water	35.6	clean with partial waterbodies	Sannel and Brown (2010), Sannel and Kuhry (2011)
ice0032009xxxx	788.1	5.0	0.85	open water	100.0	raw	Bartsch and Seifert (2012)
imc00120040725	1309.9	0.7	NA	open water	100.0	clean	this paper
ind00120090907	654.0	0.5	NA	open water	100.0	clean	this paper
kol00119650721	2382.0	5.0	NA	open water	200.0	clean	this paper
kol00219650721	2638.1	5.0	NA	open water	200.0	clean	this paper
kcp001201007xx	20.7	NA	NA	open water	1.0	clean	Walker et al. (1986), Raynolds et al. (2014)
kcp002201007xx	20.1	NA	NA	open water	1.0	clean	Walker et al. (1986), Raynolds et al. (2014)
kcp003201007xx	18.9	NA	NA	open water	1.0	clean	Walker et al. (1986), Raynolds et al. (2014)
ksl00119620628	558.8	6.0	NA	open water	144.0	clean	this paper
ksl0012012xxxx	558.8	2.5	NA	open water	25.0	clean	this paper
kur00120100805	55.5	1.0	NA	open water	4.0	clean	this paper
kur00220080926	251.5	2.5	NA	open water	187.0	clean	this paper
kyt00120070728	262.3	3.0	0.97	open water	36.0	clean	Widhalm et al. (2014a, b)
log00120110811	69.7	2.4	0.90	open water	23.0	clean	Palmtag et al. (2016)
mdn00120100716	1510.3	2.5	NA	open water	64.0	clean	this paper
mdw00120090921	1614.8	2.5	NA	open water	36.0	clean	this paper
ole00120060708	75.1	2.5	NA	open water	30.0	clean	Grosse et al. (2008)
pbp00120090813	68.6	2.5	NA	open water	12.0	clean	Muster et al. (2013)
ric001201209125	587.4	2.5	NA	open water	8.0	clean	this paper

Table 1. Continued.

Map ID	Map extent	Resolution (m)	Accuracy	Classes	Min. size (m^2)	State	Reference
rog00120070626	10.0	0.6	NA	open water	30.0	clean	Sjöberg et al. (2013)
rog00219740726	3.4	1.0	NA	open water	28.0	clean with partial waterbodies	Sannel and Kuhry (2011)
rog00220070707	3.4	0.6	NA	open water	28.0	clean with partial waterbodies	Sannel and Kuhry (2011)
rog00320070626	59.6	2.4	0.68	open water	11.0	clean	this paper
rog00420070704	62.4	2.4	0.83	open water	29.0	clean	this paper
rog00520070704	62.6	2.4	0.83	open water	11.5	clean	this paper
sam001200808xx	1.6	0.3	NA	open water	1.0	clean	Muster et al. (2012)
sei00120070706	6.7	0.6	NA	open water	30.0	clean	Sjöberg et al. (2013)
sei00220070706	82.9	2.4	0.68	open water	11.5	clean	this paper
sei00320080629	91.1	3.0	NA	open water	36.0	clean	this paper
sur00120130802	1765.6	2.0	NA	open water	16.0	clean	this paper
tav00119630831	0.8	0.5	NA	open water	28.0	clean with partial waterbodies	Sannel and Kuhry (2011)
tav00119750810	0.8	0.9	NA	open water	28.0	clean with partial waterbodies	Sannel and Kuhry (2011)
tav00120030702	0.8	1.0	NA	open water	28.0	clean with partial waterbodies	Sannel and Kuhry (2011)
tbr00120100901	694.3	2.5	NA	open water	36.0	clean	this paper
tea00120100901	462.9	2.5	NA	open water	36.0	clean	this paper
tuk00120120723	477.6	2.5	NA	open water	36.0	clean	this paper
wlc00120090825	1400.2	2.5	NA	open water, water with emersed vegetation	25.0	clean	this paper
wlc00220020801	153.8	0.6	0.89–0.95	open water	7.8	clean	Lara et al. (2015)
wlc00320090802	297.3	4.0	NA	open water	64.0	clean	Muster et al. (2013)
yak0012009xxxx	2035.5	5.0	0.85	open water	75.0	raw	Bartsch and Seifert (2012)
yam00120080824	1294.3	2.5	NA	open water	36.0	clean	this paper
yam00220100820	1006.6	2.5	NA	open water, water with emersed vegetation	100.0	clean	this paper
yfl0012011xxxx	100.0	1.0	NA	open water	4.0	clean	this paper
yuk00120090812	1078.7	2.5	NA	open water	36.0	clean	this paper
yuk00220090812	575.3	2.5	NA	open water	36.0	clean	this paper

6.2 Circum-Arctic waterbody map

6.2.1 Data set structure

The unified vector file PeRL_perma_land.shp contains the permafrost landscapes and the extrapolated waterbody statistics (Table 3). Average statistics were calculated for 10 km × 10 km boxes within large maps or when four or more maps were present in the permafrost landscapes. Average statistics are reported with their relative standard error (RE), i.e., the standard error expressed as a percentage. The permafrost landscapes are also provided as separate vector files for each region (alaska_perma_land.shp, canada_perma_land.shp, and russia_perma_land.shp) and contains the landscape characteristic of each permafrost landscape as individual attributes (Appendix B, Tables B1, B2, and B3). The unified vector file (PeRL_perma_land.shp), and the regional files can be joined using the common PERMID (Appendix B, Table B4).

6.2.2 Spatial and environmental characteristics

Altogether, we identified 230 different permafrost landscapes in the Russian lowlands, 160 in the Canadian lowlands, and 51 in the lowlands of Alaska. PeRL waterbody maps were located in 28 different permafrost landscapes (Table 4) which cover a total area of 1.4×10^6 km^2 across the Arctic; thereof

Table 2. Climate and permafrost characteristics for each study area. Latitude (lat) and longitude (long) coordinates are reported in decimal degrees (WGS84). MAAT: mean annual air temperature; TP: total precipitation; PE: permafrost extent (C – continuous, D – discontinuous, S – sporadic); PD: permafrost depth. References to all data sources are listed in Table C1.

Map ID	Country/region	Site name	Lat	Long	MAAT (°C)	TP (mm)	PE	PD (m)
abi0012010xxxx	Sweden	Abisko	68.3	19.1	0	362	S	> 16
arg00120110829, arg0022009xxxx, arg00320110711	Russia	Arga Island	73.5	123.6	−13	124	C	400–600
bar00119480804, bar00120020802, bar00120080730, bar00120100810	Alaska	Barrow Peninsula	70.9	−156.2	−11	115	C	> 400
byk00120060709	Russia	Bykovskiy Peninsula	71.8	129.3	−13	427	C	500–600
byl00120160728	Canada	Bylot Island	73.2	−80.0	−15	190	C	> 200
che00120020709, che00220090724	Russia	Cherskiy	68.8	161.6	−12	294	C	400–500
elc00120090825, elc00220020801, elc00320090802	Alaska	Elson Lagoon Coast Plain	71.2	−156.4	−11	115	C	> 400
esk00120090727	Canada	Eskimo Lakes	69.2	−133.3	−10	161	C	750
fir00120090906, fir0022009xxxx	Russia	First terrace, Lena Delta	72.9	127.3	−13	124	C	400–600
fis00120020715	Alaska	Fish–Judy Creek floodplain	70.3	−151.4	−10	97	C	260
grp00119590707, grp00120060707	Canada	Grande Rivière de la Baleine Plateau	55.3	−77.5	−4	650	S	10–50
hbl00119540701, hbl00119740617, hbl00120060706	Canada	Coastal Hudson Bay Lowlands	57.9	−94.2	−6	430	C	NA
ice0032009xxxx	Russia	Ice complex, Lena Delta	72.8	124.7	−13	124	C	400–600
imc00120040725	Alaska	Ikpikpuk middle coastal plain	70.2	−153.3	−10	97	C	260
ind00120090907, kyt00120070728	Russia	Indigirka lowlands, Kytalyk	69.7	148.8	−14	232	C	> 300
kol00119650721	Russia	Kolyma Lowland	70.0	159.1	−10	110	C	500–600
kol00219650721	Russia	Kolyma Lowland	69.5	156.3	−13	144	C	500–600
kpc001201007xx, kpc002201007xx, kpc003201007xx	Alaska	Kuparuk Coastal Plain	70.3	−148.5	−10	97	C	260
ksl00119620628, ksl0012012xxxx	Alaska	Kotzebue Sound lowlands	66.2	−165.8	−3	427	C	< 50
kur00120100805, kur00220080926	Russia	Kurungnakh, Lena Delta	72.3	126.1	−13	124	C	400–600
log00120110811	Russia	Logata	73.4	98.5	−13	270	C	NA
mdn00120100716	Canada	Mackenzie Delta north	69.1	−135.2	−8	241	D	< 100–500
mdw00120090921	Canada	Mackenzie Delta west	68.5	−134.7	−8	241	D	< 100–500
ole00120060708	Russia	Olenek channel, Lena Delta	72.9	122.9	−15	206	C	200–600
pbp00120090813	Canada	Polar Bear Pass	75.7	−98.5	−16	161	C	> 500
ric001201209125	Canada	Richards Island	69.5	−134.3	−8	241	C	> 400
rog00120070626, rog00219740726, rog00220070707, rog00320070626, rog00420070704, rog00520070704	Russia	Rogovaya	67.3	62.1	−6	538	D	ca. 50
sam001200808xx	Russia	Samoylov Island	72.4	126.5	−13	124	C	400–600
sei00120070706, sei00220070706	Russia	Seida	67.1	62.9	−6	470	D	ca. 50

Table 2. Continued.

Map ID	Country/region	Site name	Lat	Long	MAAT (°C)	TP (mm)	PE	PD (m)
sur00120130802	Russia	Surgut	62.3	74.6	−17	400	S	50–300
tav00119630831, tav00119750810, tav00120030702	Sweden	Tavvavuoma	68.5	20.9	−3	451	S	< 25
tbr00120100901, tea00120100901	Canada	Tanzin Upland Beaulieu River	62.7	−115.2	−4	289	D	NA
tuk00120120723	Canada	Tuktoyaktuk Peninsula	69.9	−130.4	−10	161	C	750
wlc00120090825, wlc00220020801, wlc00320090802	Alaska	Wainwright lower coastal plain	70.9	−156.2	−11	115	C	> 400
yak0012009xxxx	Russia	Yakutsk	62.1	130.3	−10	228	C	200–300
yam00120080824, yam00220100820	Russia	Yamal Peninsula	71.5	70.0	−6	260–400	C	100–500
yfl0012011xxxx	Alaska	Yukon Flats basin	66.2	−145.9	−5	309	D	90
yuk00120090812, yuk00220090812	Alaska	Yukon–Kuskokwim Delta	60.9	−162.4	61	471	C	100–200

1.0×10^6 km^2 are in Russia, 2.1×10^5 km^2 in Canada, and 1.7×10^5 km^2 in Alaska. About 65 % of the extrapolated area was classified as high confidence (Fig. 3). The highest landscape average areal fraction of water surface was 21 % (Fig. 4 and Table 3), and there was a waterbody density per square kilometer of 57 (Fig. 5 and Table 4).

RE of areal fraction for different subsets or maps within a permafrost landscape was about 7 % on average, with a maximum of 30 % (Table 4). RE for waterbody density was 8 % on average, with a maximum of 50 %. Our extrapolated area (1.4×10^6 km^2) represents 17.0 % of the current Arctic permafrost lowland area (below 300 m a.s.l.). PeRL provides pond and lake estimates for about 29 % (in area) of the Alaskan lowlands, 7 % of the Canadian lowlands, and 21 % of the Russian lowlands. Together all extrapolated landscapes contributed about 7 % to the current estimated Arctic permafrost area (Brown et al., 1998). In Alaska, waterbody maps were missing for permafrost landscapes with isolated permafrost (16 % of total area) or rocky lithology (36 % of total area). Dominant types of surficial geology that were not mapped include colluvial sites and sites with bedrock or of glacial origin, which together contribute 61 % to the total area. In Canada, neither isolated nor sporadic permafrost were inventoried (22 % of total area) nor was this done for areas with a ground ice content of 10–20 % or less (23 % of total area). Six of the nineteen geology classes were inventoried, which contributes 75 % to the total area. Six of seven lithology types with an areal coverage of 90 % were represented. In Russia, waterbody maps were not available in the discontinuous permafrost zone (13 % of the total area). No maps were present in regions with the geological type "deluvial–coluvial and creep" which accounts for 28 % of the total area.

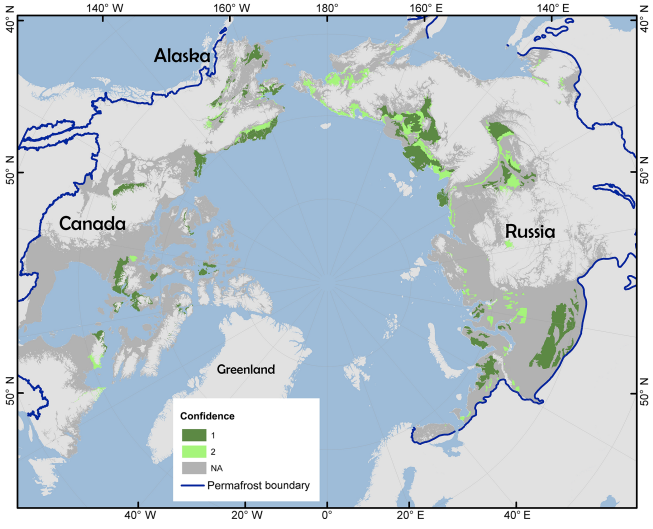

Figure 3. Confidence for permafrost lowland landscapes. Confidence class 1 (high confidence) designates permafrost landscapes where waterbody maps are available in lowland areas. Confidence class 2 (low confidence) represents permafrost landscapes with extrapolated waterbody statistics. No-value (dark grey) areas indicate that no maps were available in these permafrost landscapes. Light-grey areas indicate terrain with elevations (GTOPO 30, USGS) higher than 300 m a.s.l. which were not considered in the extrapolation. Permafrost boundary was derived from the regional databases.

7 Discussion

7.1 Classification accuracy and variability

The accuracy of the individual waterbody map depends on the spectral and spatial properties of the remote-sensing imagery employed for classification as well as the classifica-

Table 3. Attributes of ESRI shape file PeRL_perma_land.shp.

Field name	Description
PERMA_LAND	Permafrost landscape: permafrost extent/ground ice volume/surficial geology/texture
PERMID	Each permafrost landscape in the vector file is assigned a unique ID (PERMID). The first digit stands for the region (1: Alaska; 2: Canada; 3: Russia), digits 2–6 identify the single polygon, and the last three digits identify the ecozone.
AREA	Area of polygon in square meters
PERIMETER	Perimeter of polygon in square meters
Map_ID	Short ID of waterbody map used for extrapolation of statistics
confidence	1: high confidence; 2: low confidence
frac	Areal fraction of waterbodies (1.0×10^2 to 1×10^6 m^2 in surface area) in percent
frac_re	Relative standard error of areal fraction of waterbodies (1.0×10^2 m^2 to smaller than 1×10^6 m^2 in surface area) in percent
dens	Density: number of waterbodies (1.0×10^2 to 1×10^6 m^2 in surface area) per square kilometer
dens_re	Relative standard error of density of waterbodies (1.0×10^2 to 1×10^6 m^2 in surface area) in percent
frac_ponds	Areal fraction of waterbodies (1.0×10^2 m^2 to smaller than 1×10^4 m^2 in surface area) in percent
frac_po_re	Relative standard error of areal fraction of waterbodies (1.0×10^2 m^2 to smaller than 1×10^4 m^2 in surface area) in percent
dens_ponds	Ponds density: number of ponds (1.0×10^2 to 1×10^4 m^2 in surface area) per square kilometer
dens_po_re	Relative standard error of pond density (1.0×10^2 m^2 to smaller than 1×10^4 m^2 in surface area) in percent

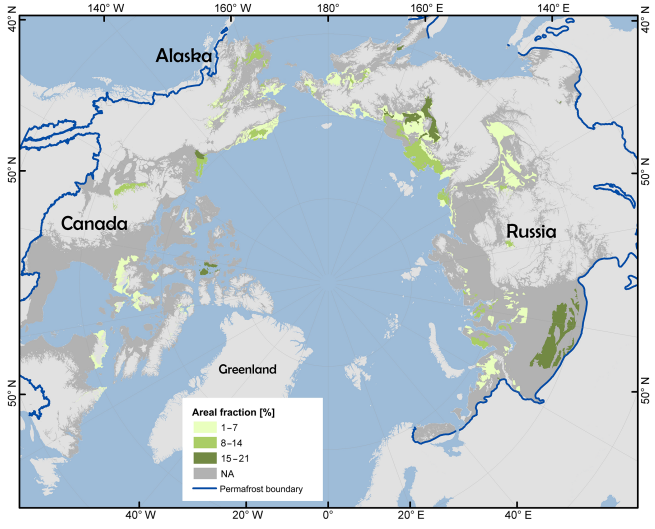

Figure 4. Areal fraction of waterbodies with surface areas between 1.0×10^2 and 1.0×10^6 m^2. Permafrost boundary was derived from the regional databases.

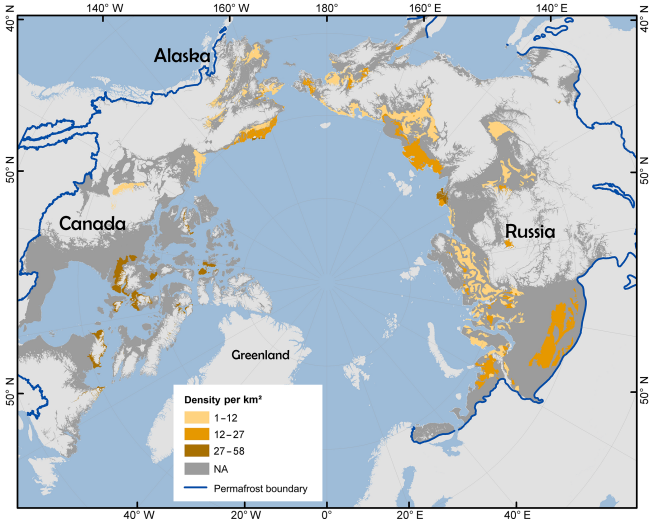

Figure 5. Waterbody density per square kilometer for waterbodies with surface areas of between 1.0×10^2 and 1.0×10^6 m^2 within permafrost landscape units. Permafrost boundary was derived from the regional databases.

tion method. In general, open-water surfaces show a high contrast to the surrounding land area in all utilized spectral bands, i.e., panchromatic, near-infrared, and X-band, since water absorbs most of the incoming radiation (Grosse et al., 2005; Muster et al., 2013). Ground surveys of waterbody surface area were available for only a few study sites. Accuracy ranged between 89 % for object-oriented mapping of multispectral imagery (Lara et al., 2015), 93 % for object-oriented mapping of panchromatic imagery (Andresen and Lougheed, 2015), and more than 95 % for a supervised maximum-likelihood classification of multispectral aerial images (Muster et al., 2012). Errors in the classification may be largely due to commission errors: i.e., the spectral signal is misinterpreted as water where in reality it may be land surface. Many shallow ponds and pond–lake margins are characterized by vegetation growing or floating in the water which cannot be adequately classified from single-band imagery (Sannel and Brown, 2010). PeRL classifications dating from early August are likely most affected since the abundance of aquatic plants peaks around that time of year. In some cases, even multispectral imagery cannot distinguish between lake and land because floating vegetation mats fully underlain by lake water may spectrally appear like a land surface (Parsekian et al., 2011).

Seasonal processes, such as snowmelt, progressing thaw depth, evaporation, and precipitation do affect the extent of surface water. Waterbody maps therefore reflect the local wa-

Table 4. Extrapolated waterbody statistics for permafrost landscapes. Permafrost extent (PE) is reported as follows: C – continuous; D – discontinuous; and S – sporadic. Extrapolated statistics include areal fraction and waterbody number per square kilometer for waterbodies ($\geq 1.0 \times 10^2$ and $\leq 1.0 \times 10^6$ m^2) and ponds ($\geq 1.0 \times 10^2$ and $< 1.0 \times 10^4$ m^2). Numbers in brackets denote the relative error in percent. The RE was calculated for 10 km × 10 km boxes within large maps or when four or more small maps could be averaged. The RE is the standard error expressed as a percentage. The standard error is the standard deviation of the sampling distribution of a statistic.

Country/region	Ecozone	PE	Ground ice (vol %)	Surficial geology	Lithology	Fraction	Density	Pond fraction	Pond density
Alaska	Arctic tundra	C	10–40	alluvial–marine	Sandy	7.3 (4.6)	17.6 (3.4)	1.6 (2.8)	16.9 (3.4)
	Arctic tundra	C	< 10	eolian, sand	Sandy	11.1 (4.9)	21.3 (10.3)	1.8 (11.4)	20.4 (10.4)
	Arctic tundra	C	> 40	glaciomarine	Silty	8 (NA)	28 (NA)	1.8 (NA)	27.3 (NA)
	Bering taiga	D	> 40	eolian, loess	Silty	10.5 (NA)	7.3 (NA)	1.1 (NA)	5.9 (NA)
	Bering taiga	S	10–40	fluvial, abandoned terrace	Silty	9.9 (5.3)	6.2 (3.8)	0.7 (3.3)	5.1 (3.9)
	Bering tundra	C	> 40	eolian, loess	Silty	5.7 (11.8)	1.6 (18)	0.3 (13.7)	1.1 (28.5)
	Intermontane boreal	D	10–40	fluvial, abandoned terrace	Silty	7.1 (NA)	2.9 (NA)	0.3 (NA)	2.4 (NA)
Canada	Northern Arctic	C	< 20	colluvial fines	Sandy Loam	15.1 (NA)	42.9 (NA)	5.9 (NA)	40.6 (NA)
	Northern Arctic	C	< 10	till veneer	NA	3.7 (NA)	57 (NA)	2.1 (NA)	50.7 (NA)
	Southern Arctic	C	> 20	glaciofluvial plain	Organic	7.6 (4.5)	5.7 (3.4)	0.5 (3)	5.3 (3.4)
	Southern Arctic	C	> 20	till blanket	Clay	13.2 (3.8)	1.9 (3.2)	0.2 (5.3)	1.0 (5.0)
	Southern Arctic	D	< 20	alluvial deposits	Loam	7.7 (6.2)	6.9 (5.3)	0.8 (5.2)	6.2 (5.4)
	Taiga plain	D	< 20	alluvial deposits	Loam	21.1 (1.4)	7.6 (1.7)	1.1 (1.8)	5.4 (2.4)
	Taiga Shield	D	< 20	till veneer	Sand	8 (13.9)	7.0 (1.9)	1.0 (1.7)	5.8 (1.2)
	Taiga Shield	D	< 20	undivided	Sand	10.8 (3.0)	2.7 (2.1)	0.3 (3.4)	1.7 (3.0)
Russia	East Siberian taiga	C	> 40	alluvial–limnetic	Coarse	5.3 (10.1)	1 (8.8)	0 (11.5)	0.7 (9.6)
	East Siberian taiga	C	> 40	alluvial–limnetic	Medium	4.9 (3.8)	2.5 (4.2)	0.4 (4.7)	2.0 (5.0)
	Northeast Siberian coastal tundra	C	> 40	alluvial–limnetic	Medium	8.3 (NA)	18.2 (NA)	0.8 (NA)	17.6 (NA)
	Northeast Siberian taiga	C	> 40	alluvial–limnetic	Organic	16.7 (10.2)	3.5 (6.3)	0.4 (5.7)	2.3 (6.4)
	Northeast Siberian taiga	C	> 40	alluvial–limnetic	Coarse	5.3 (10.1)	1 (8.8)	0 (11.5)	0.7 (9.6)
	Northeast Siberian taiga	C	> 40	cover, loess like deposits, loess and clays	Medium	1.1 (NA)	3.3 (NA)	0.2 (NA)	3.1 (NA)
	Northwest Russian Novaya Zemlya tundra	C	< 20	glacial	Medium	6.3 (28.1)	12.7 (21.4)	1.4 (24.6)	11.5 (21.5)
	Taimyr–Central Siberian tundra	C	> 40	alluvial–limnetic	Organic	10.3 (10.5)	38.8 (50.1)	2.1 (27.5)	37.8 (51.3)
	Taimyr–Central Siberian tundra	C	20–40	alluvial–limnetic	Organic	7.2 (NA)	23.8 (NA)	2.5 (NA)	23.1 (NA)
	Taimyr–Central Siberian tundra	C	20–40	glacial	Medium	3.6 (NA)	4.5 (NA)	0.4 (NA)	4.1 (NA)
	West Siberian taiga	S	20–40	organic deposits	Organic	16.7 (2.2)	20.2 (2.1)	3 (2.4)	17.6 (2.2)
	Yamal–Gydan tundra	C	> 40	marine	Medium	8.9 (5.0)	3.6 (3.1)	0.4 (2.9)	2.7 (3.2)
	Yamal–Gydan tundra	C	20–40	marine	Banded	6.1 (2.3)	8.6 (2.7)	0.8 (2.7)	7.8 (2.7)

ter balance at the time of image acquisition. Seasonal reduction in surface water extent, however, is largest in the first 2 weeks following snowmelt (Bowling et al., 2003). All PeRL maps date from the late summer season so that snowmelt and the early summer season are excluded. Changes of water extent in late summer are primarily due to evaporation and precipitation. In a study area on the Barrow Peninsula, Alaska, we find that the open-water extent varies between 6 and 8 % between the beginning and end of August of different years. However, the effect is hard to quantify as other factors such as spectral properties and resolution also impact classifications of different times at the same site. Seasonal variations may be larger in the case of heavy rain events right before image acquisition but ultimately depend on local conditions which control surface and subsurface runoff.

7.2 Uncertainty of circum-Arctic map

Uncertainties regarding the extrapolation of waterbody distributions arise from (i) the combination of different waterbody maps, (ii) the accuracy of the underlying regional permafrost maps, and (iii) the level of generalization inherent in the permafrost landscape units.

Waterbody statistics of permafrost landscapes are derived from diverse remote-sensing imagery. Imagery dates from different years and months and features different image properties. However, the effect of seasonal variability or image properties on the average statistic is small compared to the natural variability within and between permafrost landscape units.

Permafrost landscapes present a unified circum-Arctic categorization to upscale waterbody distributions. Due to the uncertainty and scale of the regional PLM, however, it cannot be expected that nonoverlapping waterbody maps within the same permafrost landscape have the same size distribution. The regional PLM are themselves extrapolated products where finite point sources of information have been used to describe larger spatial domains. No error or uncertainty measure, however, was reported for the regional maps. In addition, the variables used to describe permafrost landscapes present the dominant classes within the landscape unit. Thus, certain waterbody maps may represent landscape subtypes that are not represented by the reported average statistic. For example, two permafrost landscapes have been classified in the Lena Delta in northern Siberia. The southern and eastern parts of the delta are characterized by continuous permafrost with ground ice volumes larger than 40 %, alluvial–limnetic deposits, and organic substrate. Local studies differentiate this region further based on geomorphological differences and ground ice content. The yedoma ice complex in the southern part features a much higher ground ice content of up to 80 % and higher elevations than the eastern part; this is, however, not resolved in the Russian PLM. These subregional landscape variations are also reflected in the waterbody size distributions which are significantly different for the southern and eastern part of the delta. In the averaged statistics this is indicated by a high relative error of 11 and 28 % for the areal fraction of waterbodies and ponds, respectively, and of about 50 % for waterbody density estimates. In this case, the permafrost landscape unit in that area does not adequately reflect the known distribution of ground ice and geomorphology and demonstrates the need to further improve PLM in the future.

7.3 Potential use of database and future development

Waterbody maps and distribution statistics are the most accurate at site level. On this scale, maps can be used as a baseline to detect changes in surface inundation for seasonal, interannual, and decadal periods. Site-level size distributions can also be used to validate statistical extrapolation methods which have previously been used to extrapolate from coarser databases to finer scales (Downing et al., 2006; Seekell et al., 2010). Validation of these approaches has questioned the validity of power laws for smaller lakes and ponds but has also been limited to waterbodies as small as 1.0×10^4 m^2, i.e., 2 orders of magnitude larger than the minimum size in PeRL data sets.

The circum-Arctic map provides spatially extrapolated information for larger-scale applications. Coarse-scale global databases such as the Global Lakes and Wetlands database (GLWD) by Lehner and Döll (2004) are used in global Earth system models to represent the water fraction in model grid cells (Wania et al., 2013). The GLWD renders a reliable inventory of lakes larger 1 km^2 (Lehner and Döll, 2004). Compared to the GLWD, PeRL inventoried up to 21 % additional waterbody area. Moreover, ponds are the most frequent waterbody type (45–99 %). In light of the observed scaling of biogeochemical processes with waterbody surface area (Wik et al., 2016), PeRL results emphasize the need to include waterbodies of 1.0×10^6 m^2 and smaller in conjunction with their size distributions in physical and biogeochemical models of the high-latitude surface. Moreover, the combination of waterbody size distributions with landscape properties can motivate further study for process-based predictive simulations both on the site and regional scale. However, users should be aware of the map's uncertainty when using it to upscale landscape properties such as methane or heat fluxes. For this purpose, users should refer to the reported spatial variability, confidence class, and extensive metadata.

PeRL's permafrost landscape units represent the least common denominator across the Arctic where landscape properties have been strongly generalized. More detailed information about landscape properties was available for the Canadian database and northern Alaska (Jorgensen et al., 2014) but not for central and southern Alaska or Russia. We suggest that more detailed and accurate classes of ground ice as well as further refinement of physiography within the broad lowland zone will likely explain differences in waterbody distributions between different maps in the same permafrost

landscape. Regionally different methodologies currently prohibit a comparison of permafrost landscapes between regions and extrapolation across regions. The harmonization of landscape properties, delineation of common terrain units, and extrapolation methods for the whole Arctic require a coordinated circum-Arctic effort.

Our extrapolated area (1.4×10^6 km^2) represents only 7.0 % of the current estimated Arctic permafrost area (Brown et al., 1998) but about 17 % of the current Arctic permafrost lowland area (below 300 m a.s.l.) where most of the Arctic lakes are located (Lehner and Döll, 2004; Smith et al., 2007; Grosse et al., 2013). With a few exceptions, the reported sites are predominantly located in coastal areas. In particular, the lake-rich permafrost lowlands of Canada and central Siberia are underrepresented, despite their large spatial coverage. Underrepresented landscape types are areas with discontinuous, isolated, or sporadic permafrost, as well as areas in boreal regions. PeRL maps are conservative estimates of surface inundation as most maps capture open water only and do not include ponds smaller than 1.0×10^2 m^2 in size. PeRL maps with resolutions of less than 1 m, however, indicate the presence of many waterbodies smaller than the current threshold of 1.0×10^2 m^2. These very small waterbodies as well as water areas with emersed vegetation are highly productive environments that require attention in future mapping efforts.

8 Data availability

Waterbody maps, study area boundaries, and maps of regional permafrost landscapes including a link to detailed metadata are available at https://doi.pangaea.de/10.1594/PANGAEA.868349 (Muster et al., 2017).

9 Conclusions

PeRL maps and statistics provide a great resource for a large suite of applications across the Arctic such as resource and habitat management, hydrological and ecological modeling, pond and lake change detection, and upscaling of biogeochemical processes. PeRL maps includes waterbodies with surface areas as small as 1.0×10^2 m^2; this complements available global databases and increases waterbody size resolution by 2–4 orders of magnitude. Ponds, i.e., waterbodies with surface areas smaller than 1.0×10^4 m^2 are the dominant waterbody type found in all study areas across the Arctic. This demonstrates the need to include small waterbodies and parameterize size distributions in global land surface models. Furthermore, PeRL presents a baseline that allows future studies to investigate the direction and magnitude of past and future Arctic surface inundation. The current compilation of high-resolution waterbody maps underlines the need to produce more: vast areas in all regions are still unmapped regarding small waterbodies, especially the Canadian lowlands and boreal regions of Russia. Future mapping efforts should therefore focus equally on filling gaps and monitoring inventoried sites. The combination of waterbody statistics and landscape properties has great potential to improve our understanding of environmental drivers of surface inundation in permafrost lowlands. However, permafrost landscape maps need to be improved by increasing the level of detail as well by harmonizing mapping and extrapolation approaches across Arctic regions.

Appendix A: Image processing and subgrid sampling

A1 Processing of TerraSAR-X imagery

Geocoded EEC products obtained from the German Space Agency (DLR) are delivered in radar brightness. They are projected to the best available digital elevation model (DEM), i.e., Shuttle Radar Topography Mission (SRTM) X-band DEMs (30 m resolution) and SRTM C-band DEMs (90 m resolution). For the remaining areas, the 1 km resolution Global Land One-kilometer Base Elevation Project (GLOBE) DEM is used. The EEC is a detected multi-look product with reduced speckle and approximately square cells on the ground. The slant-range resolution of the image is 1.2 m, which corresponds to 3.3–3.5 m projected on the ground for incidence angles between 45 and 20° and an azimuth resolution of 3.3 m (Eineder et al., 2008). SSC were geocoded to the Data User Element(DUE) Permafrost DEM, and no multi-looking was applied.

A2 Subgrid sampling

In large study areas we performed a subgrid analysis, i.e., we selected waterbodies within equally sized boxes and averaged statistics from all boxes of the study area. In order to determine a representative box size, we compared the variability of waterbody distribution statistics within three study areas in Russia, Canada, and Alaska. In each study area, we selected waterbodies from a minimum of 5 and up to 50 randomly distributed boxes with varying sizes of 5 km × 5 km, 10 km × 10 km, and 20 km × 20 km. We calculated the standard error (SE) of the mean of all statistics across all boxes of the same size. SE of density (waterbody number per square kilometer) and waterbody mean surface area was lowest for 10 km × 10 km boxes. SE increased for 20 km × 20 km boxes, which is probably due to the significantly lower number of boxes that could be sampled. Only 12 PeRL sites have a study area larger than 1000 km^2 that would allow sampling a minimum of five boxes of 20 km × 20 km in size. A box size of 10 km × 10 km allows the subsampling of 26 sites with a minimum of five boxes. Taking into account the overall variability of distributions and the possible number of subgrid samples, a box size of 10 km × 10 km was chosen for subgrid analysis. Subgrid analysis was conducted for study areas larger than 300 km^2.

Table A1. Metadata about image processing and classification. PREP: preprocessing steps; bands used for classification with their corresponding spectral range; POP: post-processing steps (ME: manual editing, includes removal of rivers, streams, partial lakes, shadows, streets and gap-filling).

Map ID	Imagery	Software	PREP	Band(s)	Spectral range	Method	POP	Reference
abi0012010xxxx	orthophoto (Lantmäteriet, I2014/00691); SPOT-5; DEM	GDAL, SAGA GIS, Orfeo toolbox	1. image segmentation using orthophoto RGB (1 m) and DEM (2 m), minimum object size 130 m^2 2. classification of watermask: SVM classifier using red band and slopes	red (1 m) + slope (2 m)	610–680 nm	segmentation → SVM	ME	this paper
arg00120110829	KOMPSAT-2	ENVI 4.8, ArcGIS 12	georeferencing	NIR	760–900 nm	density slice	ME	this paper
arg0022009xxxx, fir0022009xxxx, ice0032009xxxx	RapidEye	NA	georeferencing, histogram matching routine for radiometric normalization, mosaicking	B, G, R, RE, NIR	blue: 440–510 nm, green: 520–590 nm, red: 630–685 nm, RE: 690–730 nm, NIR: 760–850 nm	object-oriented classification	NA	Bartsch and Seifert (2012)
arg00320110711	KOMPSAT-2	ENVI 4.8, ArcGIS 10	georeferencing	NIR	760–900 nm	density slice	ME	this paper
bar00119480804	aerial imagery	ENVI 4.4	co-registration and orthorectification using an image-to-image correction (RMSE of 1.0 m)	PAN	NA	object-oriented classification	ME	Andresen and Lougheed (2015)
bar00120020802	Quickbird	ENVI 4.4	co-registration and orthorectification using an image-to-image correction (RMSE of 1.0 m)	PAN	445–900 nm	object-oriented classification	ME	Andresen and Lougheed (2015)
bar00120080730	Quickbird	ENVI 4.4	co-registration and orthorectification using an image-to-image correction (RMSE of 1.0 m)	PAN	445–900 nm	object-oriented classification	ME	Andresen and Lougheed (2015)
bar00120100810	WorldView-2	ENVI 4.4	co-registration and orthorectification using an image-to-image correction (RMSE of 1.0 m)	PAN	450–800 nm	object-oriented classification	ME	Andresen and Lougheed (2015)
byk00120060709	SPOT-5	ArcGIS	georeferenced to topographic maps of scale 1 : 100 000	PAN	480–710 nm	density slice	ME	Lara et al. (2015)
byl00120160728	Pleiades-1B	Geomatica 2015, ArcGIS 10.4	pan-sharpening, orthorectification	B, G, R, NIR	430–550, 490–610, 600–720, 750–920 nm	unsupervised *k*-means classification	ME	this paper
che00120020709	IKONOS-2	ArcGIS	orthorectification	PAN	760–850 nm	density slice	ME	Grosse et al. (2008)
che00220090724	ALOS PRISM	NA	NA	PAN	520–770 nm	density slice	ME	Widhalm et al. (2014a, b)
elc00120090825, wlc00120090825	TerraSAR-X	ENVI 4.4	gamma filter (11 × 11 pixel)	X	wavelength 31 mm, frequency 9.6 GHz	unsupervised *k*-means classification	ME	this paper
elc00220020801, wlc00220020801	Quickbird	ArcGIS 10.2, eCognition 9.1	principle component analysis on raster bands, pan-sharpening	R, B, G, IR	450–520, 560–600, 630–690, 760–890 nm	object-oriented classification	ME	Lara et al. (2015)
elc00320090802, wlc00320090802	KOMPSAT-2	ENVI 4.8, ArcGIS 10	georeferencing	NIR	760–900 nm	density slice	ME	Muster et al. (2013)

Table A1. Continued.

Map ID	Imagery	Software	PREP	Band(s)	Spectral range	Method	POP	Reference
elc004200808xx	Quickbird	ArcGIS 10.2, eCognition 9.2	principle component analysis on raster bands, pan-sharpening	R, B, G, IR	450–520, 560–600, 630–690, 760–890 nm	object-oriented classification	NA	Lara et al. (2015)
esk00120090727	TerraSAR-X	ENVI 4.8, ArcGIS 10	lee filter (3 × 3 pixel), gamma filter (11 × 11 pixel)	X	wavelength 31 mm, frequency 9.6 GHz	unsupervised *k*-means classification	ME	this paper
fir00120090906	KOMPSAT-2	ENVI 4.8, ArcGIS 10	georeferencing	NIR	760–900 nm	density slice	ME	this paper
fis00120020715	airborne orthorectified radar imagery (IFSAR)	ENVI 4.5	NA	PAN	bandwidth of 135 or 270 MHz	density slice	ME	Jones et al. (2013)
grp00119590707	aerial imagery	ArcGIS 10.0	scanning (1814 dpi), georeferencing (RMSE = 1.8 m (4.2 pix))	black and white	NA	manual	NA	Bouchard et al. (2014)
grp00120060707	QuickBird	ArcGIS 10.0	geometric correction (cubic convolution resampling)	PAN	450–900 nm	manual	NA	Bouchard et al. (2014)
hbl00119540701	aerial imagery	ENVI 4.5, ENVI 4.7, ArcGIS 9	resampling of pixel resolution to 0.6 m, georeferenced to QuickBird image from 2006 RMSE of 0.38–1.42	PAN	NA	manual delineation	NA	Sannel and Brown (2010), Sannel and Kuhry (2011)
hbl00119740617	aerial imagery	ENVI 4.5, ENVI 4.7, ArcGIS 9	resampling of pixel resolution to 0.6 m, georeferenced to QuickBird image from 2006 RMSE of 0.38–1.42	PAN	NA	manual delineation	NA	Sannel and Brown (2010), Sannel and Kuhry (2011)
hbl00120060706	QuickBird	ENVI 4.5, ENVI 4.7, ArcGIS 9	NA	PAN	405–1053 nm	manual delineation	NA	Sannel and Brown (2010), Sannel and Kuhry (2011)
imc00120040725	QuickBird-2	ENVI 5.0, ArcGIS 10.3	orthorectification	PAN	760–850 nm	density slice	ME	this paper
ind00120090907	WorldView-1	ENVI 5.0, ArcGIS 10.3	orthorectification	PAN	400–900 nm	density slice, opening filter 3 × 3	ME	this paper
kol00119650721, kol00219650721	CORONA	ArcGIS 9	georeferencing	PAN	NA	manual delineation	NA	this paper
kpc001201007xx, kpc002201007xx, kpc003201007xx	digital true color aerial imagery	NA	NA	R, G, B	NA	manual delineation	NA	Walker et al. (1986), Raynolds et al. (2014)
ksl00119620628	Corona KH4	ENVI 4.8, ArcGIS 10	georeferencing to Landsat ETM & TM (RMSE = 10 m)	PAN	NA	density slice	ME	this paper
ksl0012012xxxx	SPOT-5	eCognition 8	principal component analysis on visible and IR bands	G, R, NIR	NA	object-oriented classification	ME	this paper

Table A1. Continued.

Map ID	Imagery	Software	PREP	Band(s)	Spectral range	Method	POP	Reference
kur00120100805	Geoeye	ENVI 4.8, ArcGIS 10	pan-sharpening, orthorectification (RMSE: 0.36 m)	NIR	760–900 nm	unsupervised *k*-means classification	ME	this paper
kur00220080926	ALOS PRISM	PCI Geomatica, ArcGIS 9	orthorectification based on own stereo DEM	PAN	520–770 nm	manual delineation	ME	this paper
kyt00120070728	ALOS PRISM	ENVI 4.8, ArcGIS 10	orthorectification based on own stereo DEM	PAN	520–770 nm	density slice	ME	Widhalm et al. (2014a, b)
log00120110811	QuickBird	ENVI 5.1	NA	NIR, R, G, B	485-830 nm	supervised maximum-likelihood classification	ME	Palmtag et al. (2016)
mdn00120090921	TerraSAR-X	ENVI 4.8, ArcGIS 10	lee filter (3 × 3 pixel), gamma filter (11 × 11 pixel)	X	wavelength 31 mm, frequency 9.6 GHz	density slice;	ME	this paper
mdn00120100716	TerraSAR-X	ENVI 4.8, ArcGIS 10	lee filter (3 × 3 pixel), gamma filter (11 × 11 pixel)	X	wavelength 31 mm, frequency 9.6 GHz	*k*-means classification: 15 classes, five iterations; classes 1–3 identified as water	ME	this paper
ole00120060708	SPOT-5	ArcGIS	georeferenced to topographic maps of scale 1 : 100 000	PAN	480–710 nm	density slice	ME	Grosse et al. (2008)
pbp00120090813	TerraSAR-X	ENVI 4.8, ArcGIS 10	gamma filter (11 × 11 pixel)	X	wavelength 31 mm, frequency 9.6 GHz	density slice	majority filter (7 × 7 pixel) to reduce spurious pixels in classification, ME	Muster et al. (2013)
ric001201209125	TerraSAR-X	ENVI 4.8, ArcGIS 10	lee filter (3 × 3 pixel), gamma filter (11 × 11 pixel)	X	wavelength 31 mm, frequency 9.6 GHz	*k*-means classification: 15 classes, five iterations; classes 2–4 were identified as water	ME	this paper
rog00120070626	QuickBird	ArcGIS	NA	PAN	760–850 nm	manual delineation	NA	Sjöberg et al. (2013)
rog00219740726	aerial imagery	ENVI 4.5, ENVI 4.7, ArcGIS 9	resampling of pixel resolution to 0.6 m, georeferenced to QuickBird image from 2007 with RMSE of 0.20–1.25,	PAN	NA	manual delineation	NA	Sannel and Kuhry (2011)
rog00220070707	QuickBird	ENVI 4.5, ENVI 4.7, ArcGIS 9	NA	PAN	760–850 nm	manual delineation	NA	Sannel and Kuhry (2011)
rog00320070626	QuickBird-2	classification in Definiens Professional 5.0, post-processing with ArcGIS	re-georeferenced using field measured GPS points	B, G, R, NIR	blue: 450–520 nm, green: 520-600 nm, red: 630–690 nm, NIR: 760–890 nm	supervised; see more in INFO_Qbird_classification_ version4.pdf	ME	this paper

Table A1. Continued.

Map ID	Imagery	Software	PREP	Band(s)	Spectral range	Method	POP	Reference
rog00420070704	QuickBird-2	classification in Definiens Professional 5.0, post-processing with ArcGIS	re-georeferenced using field measured GPS points	B, G, R, NIR	blue: 450–520 nm, green: 520–600 nm, red: 630–690 nm, NIR: 760–890 nm	supervised; see more in INFO_Qbird_classification_ version4.pd	ME	this paper
rog00520070704	QuickBird-2	classification in Definiens Professional 5.0, post-processing with ArcGIS	re-georeferenced using field measured GPS points	B, G, R, NIR	450–520, 520–600, 630–690, 760–890 nm	supervised; see more in INFO_Qbird_classification_ version4.pdf	ME	this paper
sam001200808xx	aerial imagery	ENVI 4.8, ArcGIS 10	georeferencing	NIR	NA	NA	ME	Muster et al. (2012)
sei00120070706	QuickBird	ArcGIS	NA	PAN	450–900 nm	manual delineation	NA	Sjöberg et al. (2013)
sei00220070706	QuickBird-2	classification in Definiens Professional 5.0, post-processing with ArcGIS	re-georeferenced using field measured GPS points	B, G, R, NIR	blue: 450–520 nm, green: 520–600 nm, red: 630–690 nm, NIR: 760–890 nm	supervised; see more in INFO_Qbird_classification_ version4.pdf	ME	this paper
sur00120130802	TerraSAR-X	ENVI 4.8, ArcGIS 10	orthorectification, gamma filter 10 × 10 m	X	wavelength 31 mm, frequency 9.6 GHz	threshold classification	ME	this paper
tav00119630831	aerial imagery	ENVI 4.5, ENVI 4.7, ArcGIS 9	resampling of pixel resolution to 0.6 m, georeferenced to IKONOS image from 2003 wihth RMSE of 1.28-3.31	PAN	NA	manual delineation	NA	Sannel and Kuhry (2011)
tav00119750810	aerial imagery	ENVI 4.5, ENVI 4.7, ArcGIS 9	resampling of pixel resolution to 0.6 m, georeferenced to IKONOS image from 2003 with RMSE of 0.60–2.38	PAN	NA	manual delineation	NA	Sannel and Kuhry (2011)
tav00120030702	IKONOS	ENVI 4.5, ENVI 4.7, ArcGIS 9	resampling of pixel resolution to 0.6 m	PAN	760–850 nm	manual delineation	NA	Sannel and Kuhry (2011)
tbr00120100901, tea00220100901	TerraSAR-X	ENVI 4.8, ArcGIS 10	lee filter (3 × 3 pixel), gamma filter (11 × 11 pixel)	X	wavelength 31 mm, frequency 9.6 GHz	*k*-means classification: 15 classes, five iterations	ME	this paper
tuk00120120723	TerraSAR-X	ENVI 4.8, ArcGIS 10	lee filter (3 × 3 pixel), gamma filter (7 × 7 pixel)	X	wavelength 31 mm, frequency 9.6 GHz	*k*-means classification: 15 classes, five iterations	ME	this paper
yam00120080824	TerraSAR-X	ENVI 4.8, ArcGIS 10	lee filter (3 × 3 pixel), gamma filter (7 × 7 pixel)	X	wavelength 31 mm, frequency 9.6 GHz	density slice;	ME	this paper

Table A1. Continued.

Map ID	Imagery	Software	PREP	Band(s)	Spectral range	Method	POP	Reference
yak0012009xxxx	RapidEye		georeferencing, histogram matching routine for radiometric normalization, mosaicking	B, G, R, RE, NIR	blue: 440–510 nm, green: 520–590 nm, red: 630–685 nm, RE: 690–730 nm, NIR: 760–850 nm	object-oriented classification	ME	Bartsch and Seifert (2012)
yam00220100820	TerraSAR-X	ENVI 4.8, ArcGIS 10	lee filter (3 × 3 pixel), gamma filter (11 × 11 pixel)	X	wavelength 31 mm, frequency 9.6 GHz	density slice;	ME	this paper
yfl0012011xxxx	aerial imagery	eCognition 8, ArcGIS 10.2	orthorectification	NIR, R, G, B	450–520, 560–600, 630–690, 760–890 nm	object-oriented classification	ME	this paper
yuk00120090812, yuk00220090812	TerraSAR-X	ENVI 4.8, ArcGIS 10	lee filter (3 × 3 pixel), gamma filter (11 × 11 pixel)	X	wavelength 31 mm, frequency 9.6 GHz	*k*-means classification: 15 classes, five iterations	ME	this paper

Appendix B: Mapping permafrost landscapes

B1 Alaskan permafrost landscape maps

The permafrost landscape map of Alaska reports surficial geology, mean annual air temperature (MAAT), primary soil texture, permafrost extent, ground ice volume, and primary thermokarst landforms (Jorgenson et al., 2008). A rule-based model was used to incorporate MAAT and surficial geology. Permafrost characteristics were assigned to each surficial deposit under varying temperatures using terrain–permafrost relationships and expert knowledge (Jorgenson et al., 2008b).

B2 Canadian permafrost landscape maps

The permafrost landscapes of Canada are described in the NEF. The NEF distinguishes four levels of generalization nested within each other. Ecozones represent the largest and most generalized units followed by ecoprovinces, ecoregions, and ecodistricts. Ecodistricts were delineated based mainly on differences in parent material, topography, landform, and soil development derived from the Soil Landscapes of Canada Working Group (2010) on a map scale of 1 : 3 000 000 to 1 : 1 000 000 (Ecological Stratification Working Group, 1995; Marshall et al., 1999), whereas ecoregions and ecoprovinces are generalized based mainly on climate, physiography, and vegetation. Ecodistricts were therefore chosen as the most appropriate to delineate permafrost landscapes. NEF reports the areal fraction of the underlying soil landscape units and attributes nested within each ecodistrict. The dominant fraction of surficial geology, lithology, permafrost extent, and ground ice volume was chosen to describe each ecodistrict. Ecodistricts with the same permafrost landscape type within the same ecozone were then merged to PL units.

B3 Russian permafrost landscape characterization

In Russia, information about permafrost extent, ground ice content, generalized geology, and lithology was available only as separate vector maps (Stolbovoi and McCallum, 2002). The individual maps were combined in ArcGIS 10.4 to delineate Russian permafrost landscape units similar to the Canadian and Alaskan databases. Russian ecozones were mapped using the global-scale map by Olson et al. (2001) which conforms to the Alaskan and Canadian ecozones. The geometric union of ecozone, ground ice content, and permafrost extent was calculated in ArcGIS 10.1 with the tool "intersect". Each unique combination of these three variables was to assigned the dominant fraction of geology and lithology type.

Table B1. Attributes contained in the polygon attribute table of Alaskan permafrost landscapes (alaska_textunderscore perma_land.shp).

Field name	Description	Source
ECOZONE	ecozone	AK2008
GEN_GEOL	generalized geology	AK2008
LITHOLOGY	texture	AK2008
GROUND_ICE	ground ice content (vol %)	AK2008
PF_EXTENT	permafrost extent	AK2008
PERMA_LAND	combined label of PF_EXTENT/GROUND_ICE/GEN_GEOL/LITHOLOGY	PeRL
ECOZID	ecozone ID	PeRL
PERMID	ID for each polygon in the vector file. The first digit stands for the region (1: Alaska; 2: Canada; 3: Russia), digits 2–6 identify the single polygon, and the last three digits identify the ecozone.	PeRL
AREA	area of polygon in square meters	PeRL
PERIMETER	perimeter of polygon in square meters	PeRL

Table B2. Description of attributes contained in the polygon attribute table of Canadian permafrost landscapes (canada_perma_land.shp).

Field name	Description	Source
ECOZONE	ecozone	NEF
ECOREGION	ecoregion	NEF
ECODISTRIC	ecodistrict	NEF
GEN_GEOL	dominant fraction of generalized (surficial) geology	NEF
LITHOLOGY	dominant fraction of texture	NEF
GROUND_ICE	dominant fraction of ground ice content in vol %	NEF
PF_EXTENT	dominant fraction of permafrost extent	NEF
PERMA_LAND	combined label of PF_EXTENT/GROUND_ICE/GEN_GEOL/LITHOLOGY	PeRL
ECOZID	ecozone ID	PeRL
PERMID	ID for each polygon in the vector file. The first digit stands for the region (1: Alaska; 2: Canada; 3: Russia), Digits 2–6 identify the single polygon, and the last three digits identify the ecozone.	PeRL
AREA	area of polygon in square meters	PeRL
PERIMETER	perimeter of polygon in square meters	PeRL

Table B3. Description of attributes contained in the polygon attribute table of Russian permafrost landscapes (russia_perma_land.shp).

Field name	Description	Source
ECOZONE	metadata: http://maps.tnc.org/	Olson et al. (2001), downloaded at http://maps.tnc.org/gis
GEN_GEOL	surficial geology	LRR; Stolbovoi and McCallum (2002)
LITHOLOGY	texture	LRR; Stolbovoi and McCallum (2002)
GROUND_ICE	ground ice content in vol %	LRR
PF_EXTENT	permafrost extent	LRR
PERMA_LAND	combined label of PF_EXTENT/GROUND_ICE/GEN_GEOL/LITHOLOGY	LRR
ECOZID	ecozone ID	PeRL
PERMID	ID for each polygon in the vector file. The first digit stands for the region (1: Alaska; 2: Canada; 3: Russia), digits 2–6 identify the single polygon, and the last three digits identify the ecozone.	PeRL
AREA	area of polygon in square meters	PeRL
PERIMETER	perimeter of polygon in square meters	PeRL

Table B4. Terminology for permafrost properties in the regional permafrost databases of Alaska (AK2008), Canada (NEF), and Russia (LRR).

Description	PeRL	AK2008	NEF	LRR
Ecozone	ECOZONE	NA	ecozone	NA
Surficial geology	GEN_GEOL	AGGRDEPOS	UNIT	PARROCK
Lithology	LITHOLOGY	TEXTURE	TEXTURE	TEXTUR
Permafrost extent	PF_EXTENT	PF_EXTENT	PERMAFROST	EXTENT_OF_
Ground ice	GROUND_ICE	ICECLOWASS	PERMAFROST	MIN_MAX

Appendix C: Study area attributes and references

Table C1. Metadata and references for climate data and permafrost depth. TP: total precipitation.

Map ID	Country/region	MAAT and TP period	Climate data source, station	Permafrost depth source
abi0012010xxxx	Sweden	2006–2011, 1997–2007	MAAT: Johansson et al. (2013); TP: Abisko, www.polar.se/abisko	Åkerman and Johansson (2008), Dobiński (2010)
arg00120110829, arg0022009xxxx	Russia	1999–2011	Boike et al. (2013)	Yershov et al. (1991)
bar00119480804, bar00120020802, bar00120080730, bar00120100810, wlc00120090825, wlc00220020801, wlc00320090802	Alaska	1981–2010	National Climatic Data Center (2016): Barrow W. Post–W. Rogers Airport, AK, US	Brown et al. (1980)
byk00120060709	Russia	1984–1994	Rivas-Martínez et al. (2011)	Grosse et al. (2008)
byl00120160728	Canada	NA	MAAT: Godin et al. (2016); TP: Fortier et al. (2007)	Smith and Burgess (2002)
che00120020709, che00220090724	Russia	1984–1994	Rivas-Martínez et al. (2011)	Grosse et al. (2008)
elc00120090825, elc00220020801, elc00320090802	Alaska	1981–2010	National Climatic Data Center (2016): Barrow W Post Rogers Airport, AK, US	Sellmann and Brown (1973)
esk00120090727	Canada	1981–2010	Environment Canada (2016): Tuktoyaktuk A	Taylor and Judge (1981)
fis00120020715	Alaska	1981–2010	National Climatic Data Center (2016): Kuparuk, AK, US	Jorgenson et al. (2008b)
fir00120090906, fir0022009xxxx, arg00320110711	Russia	1999–2011	Boike et al. (2013)	Yershov et al. (1991)
grp00119590707, grp00120060707	Canada	1971–2000	Bouchard et al. (2014), Environment Canada (2016)	Smith and Burgess (2002)
hbl00119540701, hbl00119740617, hbl00120060706	Canada	1971–2000	Sannel and Kuhry (2011), Environment Canada (2016)	NA
ice0032009xxxx	Russia	1999–2011	Boike et al. (2013)	Yershov et al. (1991)
ind00120090907, kyt00120070728	Russia	1961–1990	Chokurdakh WMO station 21946	NA
kol00119650721	Russia	1996–2015	Bukhta Ambarchik meteostation (WMO ID 25034)	Yershov et al. (1991)
kol00219650721	Russia	1996–2015	Andryushkino meteostation (WMO ID 25017)	Yershov et al. (1991)

Table C1. Continued.

Map ID	Country/region	MAAT and TP period	Climate data source, station	Permafrost depth source
kur00120100805, kur00220080926	Russia	1999–2011	Boike et al. (2013)	Yershov et al. (1991)
log00120110811	Russia	1961–1990	Khatanga WMO station 20891	NA
mdn00120100716	Canada	1981–2010	Environment Canada (2016): Inuvik A	Burn and Kokelj (2009)
mdw00120090921	Canada	1981–2010	Environment Canada (2016): Inuvik A	Burn and Kokelj (2009)
ole00120060708	Russia	1948–1960	Rivas-Martínez et al. (2011)	Grosse et al. (2008)
pbp00120090813	Canada	1981–2010	Environment Canada (2016): Resolute Cars	Smith and Burgess (2002)
imc00120040725, kpc001201007xx, kpc002201007xx, kpc003201007xx	Alaska	1981–2010	National Climatic Data Center (2016): Kuparuk, AK, US	NA
ric001201209125	Canada	1981–2010	Environment Canada (2016): Inuvik A	Burn (2002)
rog00120070626, rog00219740726, rog00220070707, rog00320070626, rog00420070704, rog00520070704	Russia	1961–1990	Hugelius et al. (2011); Vorkuta	Rivkin et al. (2008)
sam001200808xx	Russia	1999–2011	Boike et al. (2013)	Yershov et al. (1991)
sei00120070706, sei00220070706	Russia	NA	Sjöberg et al. (2013)	Rivkin et al. (2008)
ksl00119620628, ksl0012012xxxx	Alaska	1981–2010	National Climatic Data Center (2016): Nome Municipal Airport, AK, US	Jorgenson et al. (2008a)
sur00120130802	Russia	NA	Kremenetski et al. (2003)	Kremenetski et al. (2003)
tbr00120100901, tea00120100901	Canada	1981–2010	Environment Canada (2016), Yellowknife A	NA
tav00119630831, tav00119750810, tav00120030702	Sweden	1971–2000	Sannel and Kuhry (2011)	Sannel and Kuhry (2011)
tuk00120120723	Canada	1981–2010	Environment Canada (2016): Tuktoyaktuk A	Taylor and Judge (1981)
yak0012009xxxx	Russia	1930–2010	Fedorov et al. (2014)	Yershov et al. (1991)
yam00120080824, yam00220100820	Russia	2004–2013	Leibman et al. (2015); Morrasale	Yershov et al. (1991)
yfl0012011xxxx	Alaska	1981–2010	National Climatic Data Center (2016): Central Number 2, AK, US	Walvoord et al. (2012)
yuk00120090812, yuk00220090812	Alaska	1981–2010	National Climatic Data Center (2016): Bethel Airport, AK, US	NA

Table C2. Attributes contained in the polygon attribute table of circum-Arctic permafrost landscapes (PeRL_study_area.shp).

Field name	Description
Country	country
Map_ID	ID of individual waterbody map
Site	site name
MAAT	mean annual air temperature (°C)
TP	mean annual total precipitation (mm)
PE_DEPTH	permafrost depth (m)
Lat	latitude coordinate of polygon centroid in decimal degrees (WGS84)
Long	longitude coordinate of polygon centroid in decimal degrees (WGS84)
AREA	area of polygon in square meters
AREA_SQKM	area of polygon in square kilometers

Appendix D: Location of study areas and associated permafrost landscapes

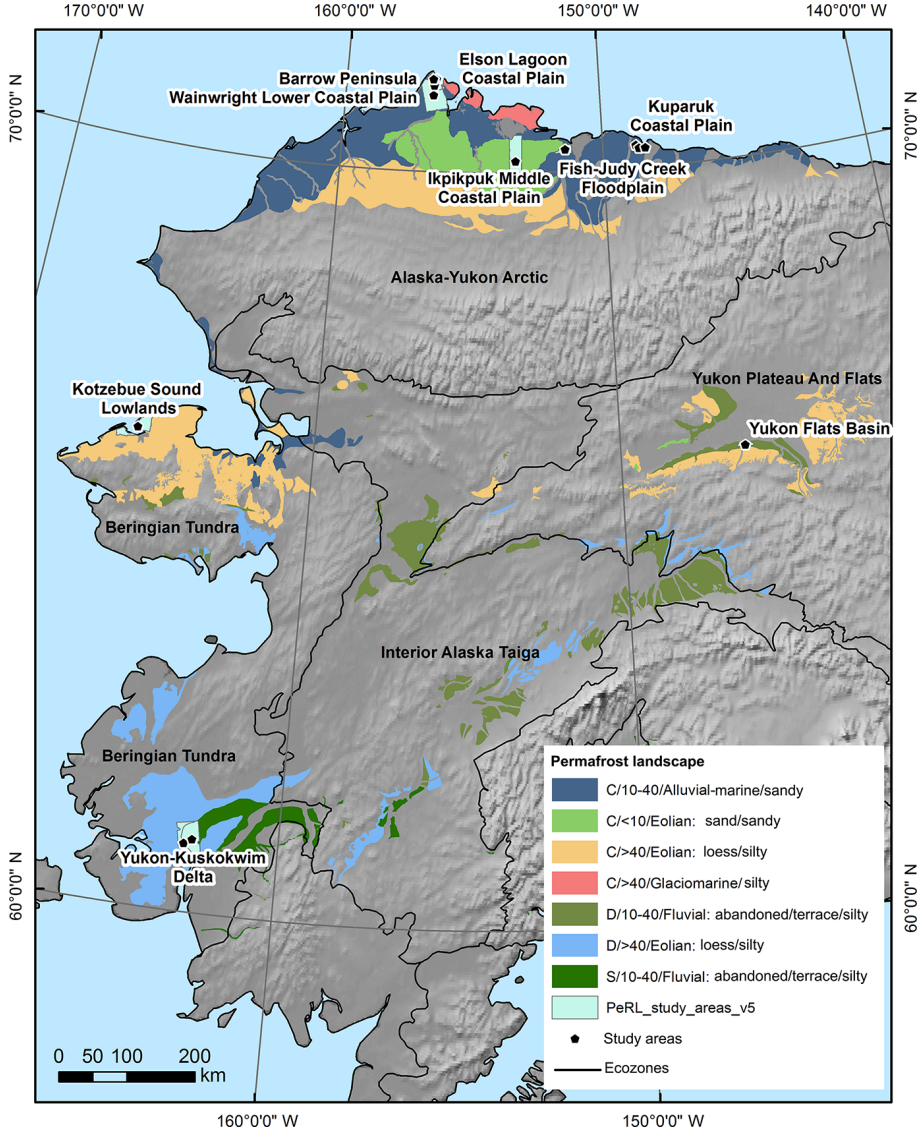

Figure D1. Study areas and associated permafrost landscapes in Alaska. Legend lists type of permafrost extent (C: continuous; D: discontinuous; S: sporadic), ground ice content (vol %), surficial geology, and lithology. Shadowed labels name study areas with waterbody maps. Black lines and labels denote ecozones.

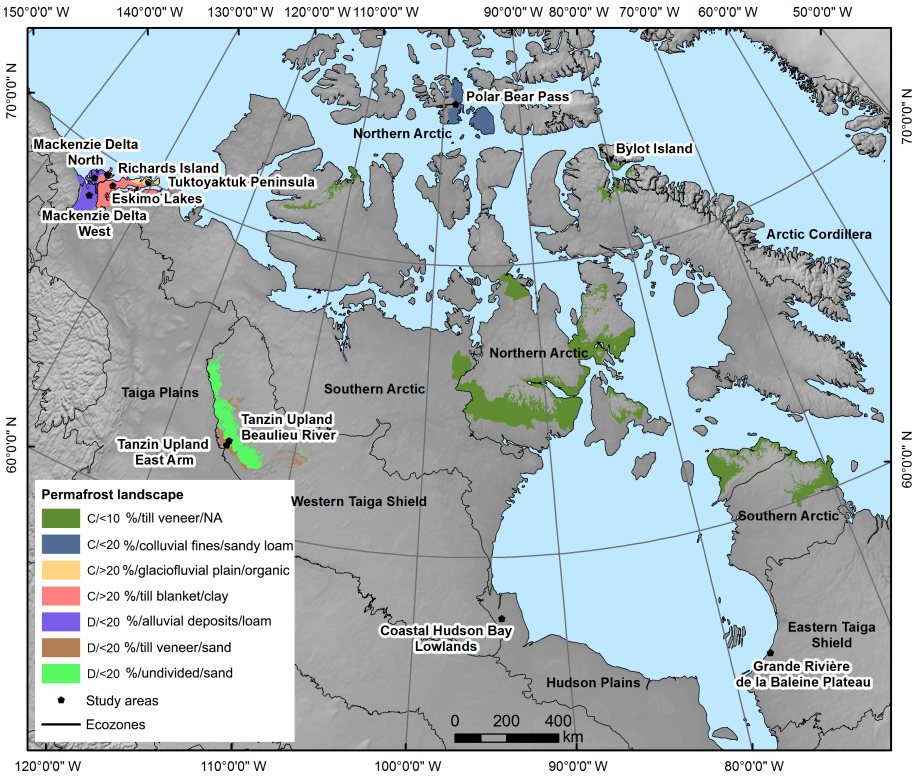

Figure D2. Study areas and associated permafrost landscapes in Canada. Legend lists type of permafrost extent (C: continuous; D: discontinuous; S: sporadic), ground ice content (vol %), surficial geology, and lithology. Shadowed labels name study areas with waterbody maps. Black lines and labels denote ecozones.

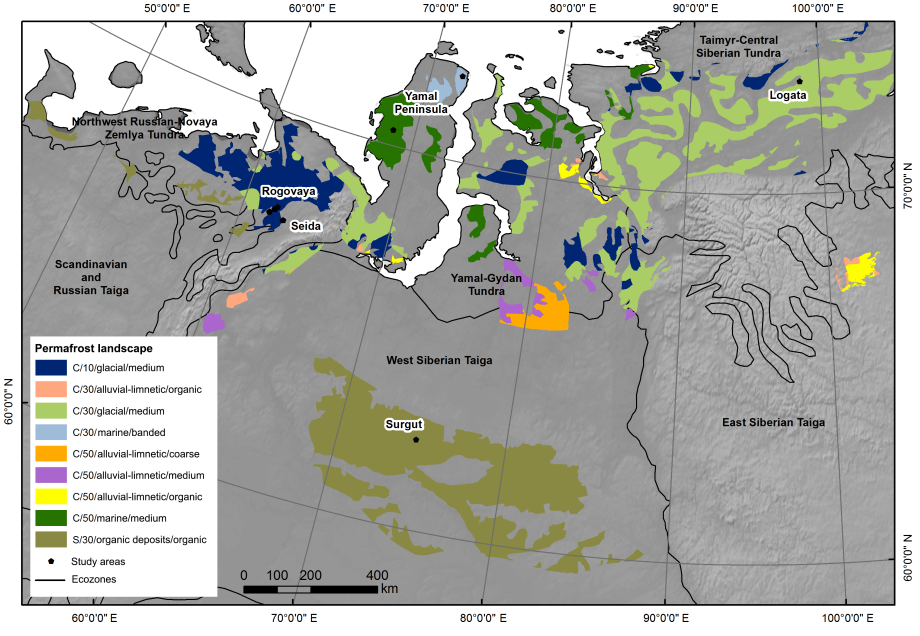

Figure D3. Study areas and associated permafrost landscapes in east Russia. Legend lists type of permafrost extent (C: continuous; D: discontinuous; S: sporadic), ground ice content (vol %), surficial geology, and lithology. Shadowed labels name study areas with waterbody maps. Black lines and labels denote ecozones.

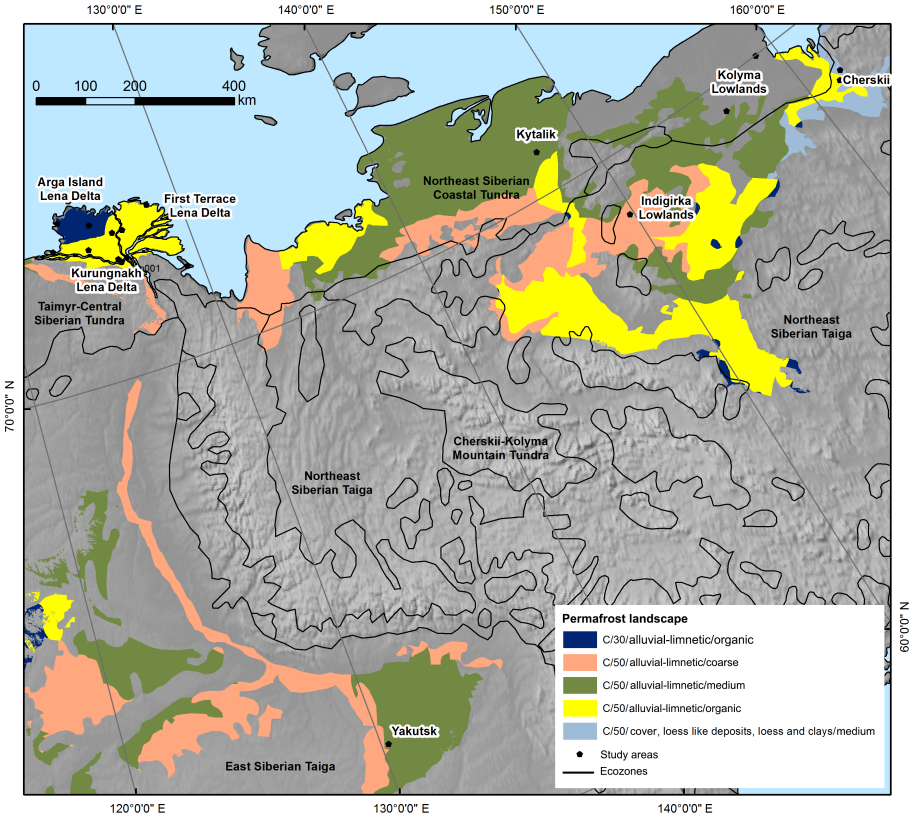

Figure D4. Study areas and associated permafrost landscapes in west Russia. Legend lists type of permafrost extent (C: continuous; D: discontinuous; S: sporadic), ground ice content (vol %), surficial geology, and lithology. Shadowed labels name study areas with waterbody maps. Black lines and labels denote ecozones.

Appendix E: Areal fraction and density for waterbody maps

Table E1. Areal fraction and density per waterbody map in Alaska. Map IDs with an asterisk were not used for extrapolation. F: areal fraction of waterbodies from $1. \times 10^2$ to 1.0×10^6 m^2 in size; REF: relative error of fraction for map subsets of 10 km × 10 km; D: waterbody density per square kilometer; RED: relative error of density; PF: pond areal fraction for waterbodies from 1.0×10^2 m^2 to smaller than 1.0×10^4 m^2; REPF: relative error of pond fraction; PoD: pond density; REPD: relative error of pond density.

Map ID	Map extent (km^2)	F (%)	REF (%)	D (no. per square kilometer)	RED (%)	PF (%)	REPF (%)	PoD (no. per square kilometer)	REPD (%)
bar00119480804*	1.9×10^1	14	NA	114	NA	8	NA	112	NA
bar00120020802*	1.9×10^1	10	NA	78	NA	5	NA	76	NA
bar00120080730*	1.9×10^1	11	NA	78	NA	6	NA	76	NA
bar00120100810*	1.9×10^1	10	NA	77	NA	6	NA	76	NA
wlc00120090825	1.4×10^3	7	5	17	3	2	3	17	3
wlc00220020801	1.5×10^2	11	NA	39	NA	3	NA	38	NA
wlc00320090802	3.0×10^2	6	NA	13	NA	1	NA	12	NA
elc00120090825	1.3×10^2	7	NA	18	NA	1	NA	17	NA
elc00220020801	1.4×10^2	9	NA	48	NA	3	NA	47	NA
elc00320090802	5.1×10^1	7	NA	18	NA	1	NA	17	NA
fis00120020715	2.4×10^2	13	NA	24	NA	2	NA	23	NA
imc00120040725	1.3×10^3	11	5	21	10	2	11	20	10
kcp001201007xx*	2.1×10^1	22	NA	49	NA	7	NA	46	NA
kcp002201007xx*	2.0×10^1	121	NA	15	NA	0	NA	1	NA
kcp003201007xx*	1.9×10^1	24	NA	58	NA	7	NA	55	NA
ksl00119620628*	5.6×10^2	11	7	12	11	1	10	11	11
ksl0012012xxxx	5.6×10^2	6	12	2	18	0	14	1	29
ycb0012011xxxx	1.0×10^2	7	NA	3	NA	0	NA	2	NA
yuk00120090812	1.1×10^3	10	5	6	4	1	3	5	4
yuk00220090812	5.8×10^2	10	NA	7	NA	1	NA	6	NA

Table E2. Areal fraction and density per waterbody map in Canada. Map IDs with an asterisk were not used for extrapolation. F: areal fraction of waterbodies from 1.0×10^2 to 1.0×10^6 m^2 in size; REF: relative error of fraction for map subsets of 10 km × 10 km; D: waterbody density per square kilometer; RED: relative error of density; PF: pond areal fraction for waterbodies from 1.0×10^2 m^2 to smaller than 1.0×10^4 m^2; REPF: relative error of pond fraction; PD: pond density; REPD: relative error of pond density.

Map ID	Map extent (km^2)	F (%)	REF (%)	D (no. per square kilometer)	RED (%)	PF (%)	REPF (%)	PD (no. per square kilometer)	REPD (%)
byl001 20160728	3.6×10^1	4	NA	51	NA	2	NA	51	NA
esk00120090727	9.2×10^2	14	4	2	3	0	4	1	5
gpr00119590707*	1.8×10^{-1}	11	NA	359	NA	11	NA	359	NA
gpr00120060707*	1.8×10^{-1}	11	NA	326	NA	11	NA	326	NA
hbl00119540701*	4.0×10	36	NA	60	NA	6	NA	57	NA
hbl00119740617*	4.0×10	38	NA	73	NA	7	NA	69	NA
hbl00120060706*	4.0×10	35	NA	60	NA	6	NA	56	NA
mdn00120100716	1.5×10^3	8	6	7	5	1	5	6	5
mdw00120090921	1.6×10^3	21	1	8	2	1	2	5	2
pbp00120090813	6.9×10^1	15	NA	43	NA	6	NA	41	NA
ric00120120925	5.9×10^2	11	8	2	10	0	12	1	11
tbr00120100901	6.9×10^2	11	3	3	2	0	3	2	3
tea00120100901	4.6×10^2	8	14	7	2	1	2	6	1
tuk00120120723	4.8×10^2	8	5	6	3	1	3	5	3

Table E3. Areal fraction and density per waterbody map in Scandinavia. Map IDs with an asterisk were not used for extrapolation. F: areal fraction of waterbodies from 1.0×10^2 to 1.0×10^6 m^2 in size; REF: relative error of fraction for map subsets of 10 km × 10 km; D: waterbody density per square kilometer; RED: relative error of density; PF: pond areal fraction for waterbodies from 1.0×10^2 m^2 to smaller than 1.0×10^4 m^2; REPF: relative error of pond fraction; PD: pond density; REPD: relative error of pond density.

Map ID	Map extent (km^2)	F (%)	REF (%)	D (no. per square kilometer)	RED (%)	PF (%)	REPF (%)	PD (no. per square kilometer)	REPD (%)
abi0012010xxxx*	3.8×10^1	6	NA	5	NA	1	NA	4	NA
tav00119630831*	8.5×10^{-1}	15	NA	40	NA	4	NA	34	NA
tav00119750810*	8.5×10^{-1}	17	NA	64	NA	7	NA	59	NA
tav00120030702*	8.5×10^{-1}	12	NA	53	NA	6	NA	50	NA

Table E4. Areal fraction and density per waterbody map in Russia. Map IDs with an asterisk were not used for extrapolation. F: areal fraction of waterbodies from 1.0×10^2 to 1.0×10^6 m^2 in size; REF: relative error of fraction for map subsets of 10 km × 10 km; D: waterbody density per square kilometer; RED: relative error of density; PF: pond areal fraction for waterbodies from 1.0×10^2 m to smaller than 1.0×10^4 m^2; REPF: relative error of pond fraction; PD: pond density; REPD: relative error of pond density.

Map ID	Map extent (km^2)	F (%)	REF (%)	D (no. per square kilometer)	RED (%)	PF (%)	REPF (%)	PD (no. per square kilometer)	REPD (%)
arg00120110829	2.0×10^2	7	NA	24	NA	2	NA	23	NA
arg0022009xxxx*	5.0×10^3	9	2	10	2	1	2	9	2
byk00120060709*	1.7×10^2	8	NA	29	NA	1	NA	28	NA
che00120020709	2.2×10^2	1	NA	3	NA	0	NA	3	NA
che00220090724	3.4×10^2	17	10	4	6	0	6	2	6
fir00120090906	1.5×10^2	9	NA	36	NA	2	NA	35	NA
arg00320110829	2.2×10^2	13	NA	19	NA	1	NA	18	NA
fir0022009xxxx*	9.8×10^3	12	4	21	4	2	4	20	4
ice0032009xxxx*	7.9×10^2	1	29	0	22	0	27	0	22
ind00120090907	6.5×10^2	5	10	1	9	0	12	1	10
kol00119659721*	2.4×10^3	6	4	2	10	0	11	2	12
kol00219659721*	2.6×10^3	7	4	1	4	0	4	1	5
kur00120100805*	5.5×10^1	8	NA	14	NA	1	NA	13	NA
kur00220080926	2.5×10^2	8	NA	6	NA	1	NA	5	NA
kyt00120070728	2.6×10^2	8	NA	18	NA	1	NA	18	NA
log00120110811	7.0×10^1	4	NA	5	NA	0	NA	4	NA
ole00120060708	7.5×10^1	11	NA	94	NA	4	NA	93	NA
rog00120070626*	1.0×10^1	19	NA	15	NA	3	NA	12	NA
rog00219740726*	3.4×10	32	NA	33	NA	3	NA	28	NA
rog00220070707*	3.4×10	26	NA	28	NA	2	NA	24	NA
rog00320070626	6.0×10^1	7	NA	11	NA	1	NA	9	NA
rog00420070704	6.2×10^1	10	NA	11	NA	2	NA	9	NA
rog00520070704	6.3×10^1	8	NA	21	NA	2	NA	19	NA
sam001200808xx*	1.6×10	14	NA	116	NA	5	NA	114	NA
sei00120070706*	6.7×10	8	NA	49	NA	4	NA	48	NA
sei00220070706	8.3×10^1	1	NA	9	NA	1	NA	8	NA
sur00120130802	1.8×10^3	17	2	20	2	3	2	18	2
yak0012009xxxx	2.0×10^3	5	4	3	4	0	5	2	5
yam00120080824	1.3×10^3	9	5	4	3	0	3	3	3
yam00220100820	1.0×10^3	6	2	9	3	1	3	8	3

Author contributions. Sina Muster compiled the database, carried out the analysis, created the figures, and wrote the paper. Stephan Lange assisted in data analysis. All authors contributed to the database compilation and assisted in the writing of the paper.

Competing interests. The authors declare that they have no conflict of interest.

Acknowledgements. This work was supported by the Helmholtz Association through a grant (VH-NG 203) awarded to Sina Muster. William J. Riley and Charles D. Koven were supported by the US Department of Energy, BER, under the NGEE-Arctic project under contract no. DE-AC02-05CH11231. Guido Grosse was supported by ERC no. 338335. Any use of trade, product, or firm names is for descriptive purposes only and does not imply endorsement by the US Government.

TerraSAR-X data of Polar Bear Pass, Canada, were acquired through the German Space Agency (DLR) via the project HYD0546. All other TerraSAR-X data in Alaska, Canada, and Russia were made available by DLR via PI agreement LAN1747 within the framework of the ESA-funded DUE GlobPermafrost project, FP7 PAGE21, and the Austrian–Russian joint FWF project COLD Yamal (I 1401). RapidEye classifications are available through the information system of the ESA DUE Permafrost project. Classifications of Rogovaya and Seida sites in Russia were conducted within the CARBONorth project (contract 036993).

Quickbird-2 and WorldView-1/-2 images (©DigitalGlobe) of Ikpikpuk middle coastal plain, Alaska, and Indigirka lowlands, Russia, were provided by the Polar Geospatial Center at the University of Minnesota through NSF AON project 1107481. The Geographic Information Network for Alaska (GINA) provided SPOT imagery of the Kotzebue Sound lowlands, Alaska.

The article processing charges for this open-access publication were covered by a Research Centre of the Helmholtz Association.

Edited by: D. Carlson
Reviewed by: two anonymous referees

References

Abnizova, A., Siemens, J., Langer, M., and Boike, J.: Small ponds with major impact: The relevance of ponds and lakes in permafrost landscapes to carbon dioxide emissions, Global Biogeochem. Cy., 26, GB2041, https://doi.org/10.1029/2011gb004237, 2012.

Åkerman, H. J. and Johansson, M.: Thawing permafrost and thicker active layers in sub-arctic Sweden, Permafrost Periglac., 19, 279–292, 2008.

Andresen, C. G. and Lougheed, V. L.: Disappearing Arctic tundra ponds: Fine-scale analysis of surface hydrology in drained thaw lake basins over a 65 year period (1948–2013), J. Geophys. Res.-Biogeo., 120, 466–479, 2015.

Bartsch, A. and Seifert, F. M.: The ESA DUE Permafrost project – A service for high latitude research, Geoscience and Remote Sensing Symposium (IGARSS), 2012 IEEE International, 22–27 July 2012, Munich, Germany, 5222–5225, https://doi.org/10.1109/IGARSS.2012.6352432, 2012.

Boike, J., Kattenstroth, B., Abramova, K., Bornemann, N., Chetverova, A., Fedorova, I., Fröb, K., Grigoriev, M., Grüber, M., Kutzbach, L., Langer, M., Minke, M., Muster, S., Piel, K., Pfeiffer, E.-M., Stoof, G., Westermann, S., Wischnewski, K., Wille, C., and Hubberten, H.-W.: Baseline characteristics of climate, permafrost and land cover from a new permafrost observatory in the Lena River Delta, Siberia (1998–2011), Biogeosciences, 10, 2105–2128, https://doi.org/10.5194/bg-10-2105-2013, 2013.

Boike, J., Grau, T., Heim, B., Günther, F., Langer, M., Muster, S., Gouttevin, I., and Lange, S.: Satellite-derived changes in the permafrost landscape of central Yakutia, 2000–2011: Wetting, drying, and fires, Global Planet. Change, 139, 116–127, https://doi.org/10.1016/j.gloplacha.2016.01.001, 2016.

Bouchard, F., Francus, P., Pienitz, R., Laurion, I., and Feyte, S.: Subarctic thermokarst ponds: Investigating recent landscape evolution and sediment dynamics in thawed permafrost of northern Québec (Canada), Arct. Antarct. Alp. Res., 46, 251–271, https://doi.org/10.1657/1938-4246-46.1.251, 2014.

Bouchard, F., Laurion, I., Preskienis, V., Fortier, D., Xu, X., and Whiticar, M. J.: Modern to millennium-old greenhouse gases emitted from ponds and lakes of the Eastern Canadian Arctic (Bylot Island, Nunavut), Biogeosciences, 12, 7279–7298, https://doi.org/10.5194/bg-12-7279-2015, 2015.

Bowling, L. C., Kane, D. L., Gieck, R. E., Hinzman, L. D., and Lettenmaier, D. P.: The Role of Surface Storage in a Low-Gradient Arctic Watershed, Water Resour. Res., 39, 1087, https://doi.org/10.1029/2002WR001466, 2003.

Brown, J., Miller, P. C., Tieszen, L. L., and Bunnell, F.: An arctic ecosystem: the coastal tundra at Barrow, Alaska, Dowden, Hutchinson & Ross, Inc., 1980.

Brown, J., Ferrians Jr., O. J., Heginbottom, J. A., and Melnikov, E. S.:. Circum-arctic map of permafrost and ground ice conditions, National Snow and Ice Data Center, Boulder, CO, Digital media, 1998 (revised February 2001).

Burn, C.: Tundra lakes and permafrost, Richards Island, western Arctic coast, Canada, Can. J. Earth Sci., 39, 1281–1298, 2002.

Burn, C. and Kokelj, S.: The environment and permafrost of the Mackenzie Delta area, Permafrost Periglac., 20, 83–105, 2009.

CAFF: Arctic Biodiversity Assessment 2013, Arctic Council, Akureyri, Iceland, 2013.

Carroll, M., Townshend, J., DiMiceli, C., Loboda, T., and Sohlberg, R.: Shrinking lakes of the Arctic: Spatial relationships and trajectory of change, Geophys. Res. Lett., 38, L20406, https://doi.org/10.1029/2011GL049427, 2011.

Dobiński, W.: Geophysical characteristics of permafrost in the Abisko area, northern Sweden, Pol. Polar Res., 31, 141–158, 2010.

Eineder, M., Fritz, T., Mittermayer, J., Roth, A., Boerner, E., and Breit, H.: TerraSAR-X Ground Segment, Basic Product Specification Document, German Aerospace Agency, Oberpfaffenhofen, Germany, 103 pp., 2008.

Fedorov, A. N., Ivanova, R. N., Park, H., Hiyama, T., and Iijima, Y.: Recent air temperature changes in the permafrost land-

scapes of northeastern Eurasia, Polar Science, 8, 114–128, https://doi.org/10.1016/j.polar.2014.02.001, 2014.

Feng, M., Sexton, J. O., Channan, S., and Townshend, J. R.: A global, high-resolution (30-m) inland water body dataset for 2000: First results of a topographic–spectral classification algorithm, International Journal of Digital Earth, 9, 113–133, 2015.

Fortier, D., Allard, M., and Shur, Y.: Observation of rapid drainage system development by thermal erosion of ice wedges on Bylot Island, Canadian Arctic Archipelago, Permafrost Periglac., 18, 229–243, https://doi.org/10.1002/ppp.595, 2007.

Godin, E., Fortier, D., and Lévesque, E.: Nonlinear thermal and moisture response of ice-wedge polygons to permafrost disturbance increases heterogeneity of high Arctic wetland, Biogeosciences, 13, 1439–1452, https://doi.org/10.5194/bg-13-1439-2016, 2016.

Grosse, G., Schirrmeister, L., Kunitsky, V. V., and Hubberten, H. W.: The use of CORONA images in remote sensing of periglacial geomorphology: an illustration from the NE Siberian coast, Permafrost Periglac., 16, 163–172, 2005.

Grosse, G., Romanovsky, V., Walter, K., Morgenstern, A., Lantuit, H., and Zimov, S.: Distribution of Thermokarst Lakes and Ponds at Three Yedoma Sites in Siberia, Ninth International Conference on Permafrost, 29 June–3 July 2008, University of Alaska, Fairbanks, USA, 551–556, 2008.

Grosse, G., Jones, B., and Arp, C. D.: Thermokarst lakes, drainage, and drained basins, in: Treatise on Geomorphology, edited by: Shroder, J., Giardino, R., and Harbor, J., Academic Press, San Diego, CA, 8, 325–353, https://doi.org/10.1016/B978-0-12-374739-6.00216-5, 2013.

Hinzman, L. D., Deal, C. J., McGuire, A. D., Mernild, S. H., Polyakov, I. V., and Walsh, J. E.: Trajectory of the Arctic as an integrated system, Ecol. Appl., 23, 1837–1868, https://doi.org/10.1890/11-1498.1, 2013.

Hugelius, G., Virtanen, T., Kaverin, D., Pastukhov, A., Rivkin, F., Marchenko, S., Romanovsky, V., and Kuhry, P.: High-resolution mapping of ecosystem carbon storage and potential effects of permafrost thaw in periglacial terrain, European Russian Arctic, J. Geophys. Res., 116, G03024, https://doi.org/10.1029/2010JG001606, 2011.

Johansson, M., Callaghan, T. V., Bosiö, J., Åkerman, H. J., Jackowicz-Korczynski, M., and Christensen, T. R.: Rapid responses of permafrost and vegetation to experimentally increased snow cover in sub-arctic Sweden, Environ. Res. Lett., 8, 035025, https://doi.org/10.1088/1748-9326/8/3/035025, 2013.

Jones, B., Grosse, G., Arp, C., Jones, M., Anthony, K. M. W., and Romanovsky, V.: Modern thermokarst lake dynamics in the continuous permafrost zone, northern Seward Peninsula, Alaska, J. Geophys. Res., 116, G00M03, https://doi.org/10.1029/2011JG001666, 2011.

Jones, B. M., Gusmeroli, A., Arp, C. D., Strozzi, T., Grosse, G., Gaglioti, B. V., and Whitman, M. S.: Classification of freshwater ice conditions on the Alaskan Arctic Coastal Plain using ground penetrating radar and TerraSAR-X satellite data, Int. J. Remote Sens., 34, 8267–8279, 2013.

Jorgenson, M., Yoshikawa, K., Kanevskiy, M., Shur, Y., Romanovsky, V., Marchenko, S., Grosse, G., Brown, J., and Jones, B.: Permafrost characteristics of Alaska, Proc. of the Ninth Inter. Conf. on Permafrost (NICOP), University of Alaska, Fairbanks, 29 June–3 July 2008, 121–122, 2008.

Klonus, S. and Ehlers, M.: Pansharpening with TerraSAR-X and optical data, 3rd TerraSAR-X Science Team Meeting, Darmstadt, Germany, 25 and 26 November 2008, 25–26, 2008.

Kravtsova, V. I. and Rodionova, T. V.: Variations in size and number of thermokarst lakesin different permafrost regions: Spaceborne evidence, Earth's Cryosphere, XX, 75–81, 2016.

Kremenetski, K. V., Velichko, A. A., Borisova, O. K., MacDonald, G., Smith, L. C., Frey, K. E., and Orlova, L. A.: Peatlands of the Western Siberian lowlands: current knowledge on zonation, carbon content and Late Quaternary history, Quaternary Sci. Rev., 22, 703–723, 2003.

Labrecque, S., Lacelle, D., Duguay, C. R., Lauriol, B., and Hawkings, J.: Contemporary (1951–2001) evolution of lakes in the Old Crow Basin, Northern Yukon, Canada: Remote sensing, numerical modeling, and stable isotope analysis, Arctic, 62, 225–238, 2009.

Langer, M., Westermann, S., Walter Anthony, K., Wischnewski, K., and Boike, J.: Frozen ponds: production and storage of methane during the Arctic winter in a lowland tundra landscape in northern Siberia, Lena River delta, Biogeosciences, 12, 977–990, https://doi.org/10.5194/bg-12-977-2015, 2015.

Lara, M. J., McGuire, A. D., Euskirchen, E. S., Tweedie, C. E., Hinkel, K. M., Skurikhin, A. N., Romanovsky, V. E., Grosse, G., Bolton, W. R., and Genet, H.: Polygonal tundra geomorphological change in response to warming alters future CO_2 and CH_4 flux on the Barrow Peninsula, Glob. Change Biol., 21, 1634–1651, 2015.

Laurion, I., Vincent, W. F., MacIntyre, S., Retamal, L., Dupont, C., Francus, P., and Pienitz, R.: Variability in greenhouse gas emissions from permafrost thaw ponds, Limnol. Oceanogr., 55, 115–133, 2010.

Lehner, B. and Döll, P.: Development and validation of a global database of lakes, reservoirs and wetlands, J. Hydrol., 296, 1–22, https://doi.org/10.1016/j.jhydrol.2004.03.028, 2004.

Leibman, M., Khomutov, A., Gubarkov, A., Mullanurov, D., and Dvornikov, Y.: The research station "Vaskiny Dachi", Central Yamal, West Siberia, Russia – a review of 25 years of permafrost studies, Fennia, 193, 3–30, 2015.

Liao, A., Chen, L., Chen, J., He, C., Cao, X., Chen, J., Peng, S., Sun, F., and Gong, P.: High-resolution remote sensing mapping of global land water, Science China Earth Sciences, 57, 2305–2316, 2014.

Liljedahl, A. K., Boike, J., Daanen, R. P., Fedorov, A. N., Frost, G. V., Grosse, G., Hinzman, L. D., Iijma, Y., Jorgenson, J. C., Matveyeva, N., Necsoiu, M., Raynolds, M. K., Romanovsky, V. E., Schulla, J., Tape, K. D., Walker, D. A., Wilson, C. J., Yabuki, H., and Zona, D.: Pan-Arctic ice-wedge degradation in warming permafrost and its influence on tundra hydrology, Nat. Geosci., 9, 312–318, https://doi.org/10.1038/ngeo2674, 2016.

Marshall, I., Schut, P., and Ballard, M.: A national ecological framework for Canada: Attribute data, Agriculture and AgriFood Canada, Research Branch, Centre for Land and Biological Resources Research, and Environment Canada, State of the Environment Directorate, Ecozone Analysis Branch, Ottawa/Hull, Canada, 1999.

Muster, S.: Decomposing Arctic Land Cover. Implications of heterogeneity and scale for the estimation of energy fluxes in Arctic tundra landscapes, Universität Heidelberg, Heidelberg, Germany, 121 pp., 2013.

Muster, S., Langer, M., Heim, B., Westermann, S., and Boike, J.: Subpixel heterogeneity of ice-wedge polygonal tundra: a multi-scale analysis of land cover and evapotranspiration in the Lena River Delta, Siberia, Tellus B, 64, 17301, https://doi.org/10.3402/tellusb.v64i0.17301, 2012.

Muster, S., Heim, B., Abnizova, A., and Boike, J.: Water body distributions across scales: A remote sensing based comparison of three Arctic tundra wetlands, Remote Sens., 5, 1498–1523, https://doi.org/10.3390/rs5041498, 2013.

Muster, S., Roth, K., Langer, M., Lange, S., Cresto-Aleina, F., Bartsch, A., Morgenstern, A., Grosse, G., Jones, B., Sannel, A. B. K., Sjöberg, Y., Günther, F., Andresen, C., Veremeeva, A., Lindgren, P. R., Bouchard, F., Lara, M. J., Fortier, D., Charbonneau, S., Virtanen, T. A., Hugelius, G., Palmtag, J., Siewert, M. B., Riley, W. J., Koven, C. D., and Boike, J.: PeRL: Permafrost Region Pond and Lake Database, links to ArcGIS shapefiles, https://doi.org/10.1594/PANGAEA.868349, 2017.

Olson, D. M., Dinerstein, E., Wikramanayake, E. D., Burgess, N. D., Powell, G. V., Underwood, E. C., D'amico, J. A., Itoua, I., Strand, H. E., and Morrison, J. C.: Terrestrial Ecoregions of the World: A New Map of Life on Earth: A new global map of terrestrial ecoregions provides an innovative tool for conserving biodiversity, BioScience, 51, 933–938, 2001.

Palmtag, J., Ramage, J., Hugelius, G., Gentsch, N., Lashchinskiy, N., Richter, A., and Kuhry, P.: Controls on the storage of organic carbon in permafrost soil in northern Siberia, Eur. J. Soil Sci., 67, 478–491, 2016.

Paltan, H., Dash, J., and Edwards, M.: A refined mapping of Arctic lakes using Landsat imagery, Int. J. Remote Sens., 36, 5970–5982, https://doi.org/10.1080/01431161.2015.1110263, 2015.

Ramsar Convention Secretariat: Designating ramsar sites: strategic framework and guidelines for the future development of the list of wetland for international importance, 4th Edn., Ramsar handbooks for the wise use of wetlands, Ramsar Convention Secretariat, Gland, Switzerland, 2010.

Rautio, M., Dufresne, F., Laurion, I., Bonilla, S., Vincent, W., and Christoffersen, K.: Shallow freshwater ecosystems of the circumpolar Arctic, Ecoscience, 18, 204–222, 2011.

Raynolds, M. K., Walker, D. A., Ambrosius, K. J., Brown, J., Everett, K. R., Kanevskiy, M., Kofinas, G. P., Romanovsky, V. E., Shur, Y., and Webber, P. J.: Cumulative geoecological effects of 62 years of infrastructure and climate change in ice-rich permafrost landscapes, Prudhoe Bay Oilfield, Alaska, Glob. Change Biol., 20, 1211–1224, https://doi.org/10.1111/gcb.12500, 2014.

Rivas-Martínez, S., Rivas-Sáenz, S., and Penas, A. S.: Worldwide bioclimatic classification system, Global Geobotany, 1, 1–634, https://doi.org/10.5616/gg110001, 2011.

Rivkin, F., Vlasova, J., Popova, A., Mazhitova, G., Kuhry, P., Parmuzin, I., and Chehina, I.: Mesoscale and detailed geocryological mapping as a basis for carbon budget assessment (East European Russian Arctic, CARBO-North project), Proc. of the Ninth Inter. Conf. on Permafrost (NICOP), University of Alaska, Fairbanks, 29 June–3 July 2008, 1493–1498, 2008.

Sannel, A. B. K. and Brown, I. A.: High-resolution remote sensing identification of thermokarst lake dynamics in a subarctic peat plateau complex, Can. J. Remote Sens., 36, S26–S40, https://doi.org/10.5589/m10-010, 2010.

Sannel, A. B. K. and Kuhry, P.: Warming-induced destabilization of peat plateau/thermokarst lake complexes, J. Geophys. Res., 116, G03035, https://doi.org/10.1029/2010JG001635, 2011.

Schuur, E. A. G., Bockheim, J. G., Canadell, J. G., Euskirchen, E. S., Field, C. B., Goryachkin, S. V., Hagemann, S., Kuhry, P., Lafleur, P. M., Lee, H., Mazhitova, G., Nelson, F. E., Rinke, A., Romanovsky, V. E., Shiklomanov, N., Tarnocai, C., Venevsky, S., Vogel, J. G., and Zimov, S. A.: Vulnerability of Permafrost Carbon to Climate Change: Implications for the Global Carbon Cycle, BioScience, 58, 701–714, https://doi.org/10.1641/B580807, 2008.

Sellmann, P. V. and Brown, J.: Stratigraphy and diagenesis of perennially frozen sediments in the Barrow, Alaska, region, in: Permafrost, the North American Contribution to the Second International Conference, National Academy of Sciences, Washington, DC, 171–181, 1973.

Sjöberg, Y., Hugelius, G., and Kuhry, P.: Thermokarst lake morphometry and erosion features in two peat plateau areas of northeast European Russia, Permafrost Periglac., 24, 75–81, 2013.

Smith, L. C., Sheng, Y., and MacDonald, G. M.: A First Pan-Arctic Assessment of the Influence of Glaciation, Permafrost, Topography and Peatlands on Northern Hemisphere Lake Distribution, Permafrost Periglac., 18, 201–208, https://doi.org/10.1002/ppp.581, 2007.

Stolbovoi, V. and McCallum, I.: Land Resources of Russia, International Institute for Applied Systems Analysis and the Russian Academy of Science, Laxenburg, Austria, 2002.

Taylor, A. E. and Judge, A. S.: Measurement and prediction of permafrost thickness, Arctic Canada, Energy, Mines and Resources Canada, Earth Physics Branch, Ottawa, Canada, 1981.

Veremeeva, A. A. and Glushkova, N. V.: Formation of relief in the regions of Ice Complex deposits distribution: remote sensing and GIS studies in the Kolyma lowland tundra, Earth's Cryosphere, XX, 15–25, 2016.

Verpoorter, C., Kutser, T., Seekell, D. A., and Tranvik, L. J.: A global inventory of lakes based on high-resolution satellite imagery, Geophys. Res. Lett., 41, 6396–6402, https://doi.org/10.1002/2014GL060641, 2014.

Walker, D. A., Webber, P. J., Walker, M. D., Lederer, N. D., Meehan, R. H., and Nordstrand, E. A.: Use of geobotanical maps and automated mapping techniques to examine cumulative impacts in the Prudhoe Bay Oilfield, Alaska, Environ. Conserv., 13, 149–160, 1986.

Walvoord, M. A., Voss, C. I., and Wellman, T. P.: Influence of permafrost distribution on groundwater flow in the context of climate-driven permafrost thaw: Example from Yukon Flats Basin, Alaska, United States, Water Resour. Res., 48, W07524, https://doi.org/10.1029/2011WR011595, 2012.

Watts, J., Kimball, J., Jones, L., Schroeder, R., and McDonald, K.: Satellite Microwave remote sensing of contrasting surface water inundation changes within the Arctic–Boreal Region, Remote Sens. Environ., 127, 223–236, 2012.

Watts, J. D., Kimball, J. S., Bartsch, A., and McDonald, K. C.: Surface water inundation in the boreal-Arctic: potential impacts on regional methane emissions, Environ. Res. Lett., 9, 075001, https://doi.org/10.1088/1748-9326/9/7/075001, 2014.

Widhalm, B., Hogström, E., Ressl, C., Trofaier, A., Heim, B., Biasi, C., and Bartsch, A.: PAGE21 WP5-Land surface hydrology from remotely sensed data at PAGE21 sites, Department of Geodesy

and Geoinformation (GEO), Research Groups Photogrammetry and Remote Sensing, Vienna University of Technology, Vienna, Austria, 15 pp., 2014a.

Widhalm, B., Högström, E., Ressl, C., Trofaier, A. M., Heim, B., Biasi, C., and Bartsch, A.: Land surface hydrology from remotely sensed data at PAGE21 sites with links to geotiff images, https://doi.org/10.1594/PANGAEA.834200, 2014b.

Wik, M., Varner, R. K., Anthony, K. W., MacIntyre, S., and Bastviken, D.: Climate-sensitive northern lakes and ponds are critical components of methane release, Nat. Geosci., 9, 99–105, https://doi.org/10.1038/ngeo2578, 2016.

Yershov, E. D., Kondrat'yeva, K. A., KLoginov, V. F., and Sychev, I. K.: Geocryological Map of Russia and Neighbouring Republics, Faculty of Geology, Chair of Geocryology, Lomonosov Moscow State University, Moscow, Russia, 1991.